International Geology Review, Vol. 45, 2003, p. 263–286.

Geochemistry of Mesozoic Mafic Rocks Adjacent to the Chenzhou-Linwu fault, South China: Implications for the Lithospheric Boundary between the Yangtze and Cathaysia Blocks

YUEJUN WANG,[1] WEIMING FAN, FENG GUO, TOUPING PENG, AND CHAOWEN LI
Guangzhou Institute of Geochemistry, Chinese Academy of Sciences, Guangzhou 510640, China

Abstract

To constrain the Mesozoic tectonic evolution and the lithospheric boundary between the Yangtze and Cathaysia blocks in South China, we present geochronological and geochemical data for Mesozoic basaltic lavas and related mafic dikes west (Group 1) and east (Group 2) of the Chenzhou-Linwu fault. Three episodes of mafic magmatism around the Chenzhou-Linwu fault were identified: ca.175 Ma, 125–150 Ma, and 80–95 Ma, respectively. Group 1 rocks (alkaline basanite and trachybasalt), with ages of >125 Ma, have a wide range of $^{87}Sr/^{86}Sr(t)$ values (0.7035–0.7069), and $\varepsilon_{Nd(t)}$ values (–3.75 to + 6.10). In contrast, Group 2 rocks (subalkaline basalt and basaltic andesite), with ages of > 125 Ma, exhibit $^{87}Sr/^{86}Sr(t)$ values of 0.7075–0.7087 and $\varepsilon_{Nd(t)}$ values of –2.04 to + 1.05. Both groups are strongly enriched in incompatible elements, with variable negative Nb-Ta anomalies. However, Group 1 rocks commonly have higher LREE and Ba/Nb, Rb/Nb, Ba/Th, and Ba/La ratios and lower Th/Nb, Th/La, and Zr/Nb ratios than Group 2 rocks. Rocks with ages of 80–95 Ma from both groups have very similar elemental and isotopic compositions ($^{87}Sr/^{86}Sr(t)$ = 0.7033–0.7052, εNd(t) = +3.99 to + 8.00), consistent with those of OIB.

Strong coupling between incompatible elemental ratios and isotopes suggests that Group 1 rocks might have been derived from an EMI-like continental lithospheric mantle with an OIB source. In contrast, Group 2 rocks come from an EMII-like mantle source contaminated by an OIB component. We conclude that Mesozoic mafic rocks with ages of >125 Ma originated chiefly from an enriched lithospheric mantle heated by ascending asthenosphere, whereas the mafic rocks with ages of ca. 80–95 Ma were derived from upwelling asthenospheric mantle in response to intra-continental lithospheric extension in the South China interior. The spatial variations of EMI- and EMII-like source signatures for Mesozoic mafic rocks around the Chenzhou-Linwu fault suggest that the fault represents the Mesozoic lithospheric boundary between the Yangtze and Cathaysia blocks. The Jinxian-Anhua fault was only a near-surface boundary between the sutured blocks. The crust of the Cathaysia block might have been thrust westward over the Yangtze block with a displacement of >400 km at a time no later than ca. 175 Ma. A model for crustal detachment collision (>ca. 175 Ma) and subsequent intra-continental lithospheric extension (175–80 Ma) is proposed for the Mesozoic tectonic evolution of South China.

Introduction

OVER THE PAST 20 years, several Mesozoic tectonic models have been postulated to account for the Mesozoic tectonic evolution of the South China Block (SCB) (Hsü et al., 1990; Charvet et al., 1994; Zhou and Li, 2000; Li, 2000). Some models, such as an Andean-type active continental margin, Alps-type collision belt and lithospheric subduction with underplating of mafic magma, suggest that the tectonic regime was dominantly compressive as the result of either westward subduction of a Mesozoic Pacific plate, or the closure of an oceanic basin in the SCB interior (Holloway, 1982; Hsü et al., 1990; Faure et al., 1996; Zhou and Li, 2000). Alternatively, wrench faulting (Xu et al., 1993) and continental rifting and extension (Gilder et al., 1996; Li, 2000; Li et al., 2003; Wang et al., 2002, 2003) models have postulated that intracontinental lithospheric extension and thinning dominated since the early Mesozoic. Major debates among proponents of these models are focused on whether Mesozoic mag-

[1]Corresponding author; email: yjwang@gig.ac.cn

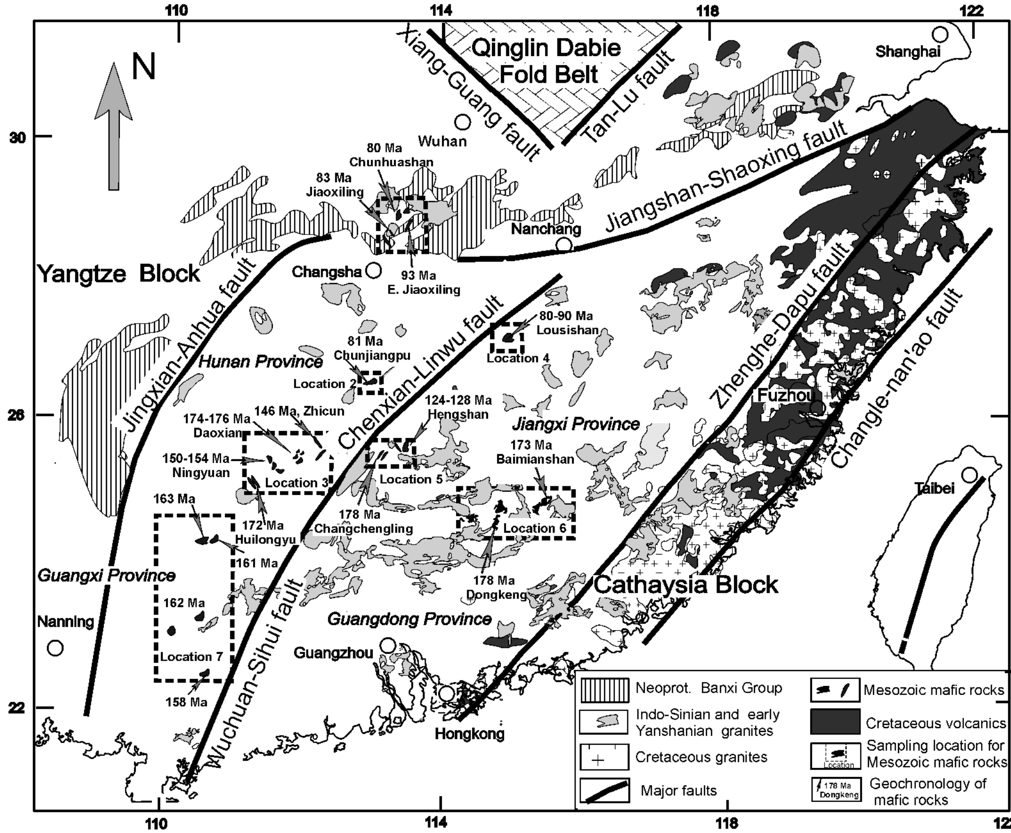

FIG. 1. Sketch tectonic map (Locations 1–7) with distribution of Mesozoic mafic rocks in SCB. The boundary between the Yangtze and Cathaysia blocks was previously defined by the occurrence of the Neoproterozoic Banxi Group, corresponding to the Jinxian-Anhua fault (Chen and Jahn, 1998). Location 7 is from Li et al. (2003).

matic activity represents post-Indosinian magmatism related to lithospheric extension, or constitutes arc magmatism associated with subduction/collision. Answering this question is the key for achieving a better understanding of the Mesozoic tectonic evolution of the SCB (Rowley et al., 1989; Li, 2000; Li et al. 2003).

Among these models, the Neoproterozoic Banxi Group is considered by the authors to define the boundary between Yangtze craton and the outboard Cathaysia block (Hsü et al., 1990; Chen and Jahn, 1998) (Fig. 1). For example, in the Alpine-type collision model (Hsü et al., 1990), the Banxi Group was interpreted as a Triassic mélange and a long displaced thrust-fold sheet. However, the definition of the boundary in this model was mainly based on near-surface structures rather than on lithospheric mapping (O'Reilly and Griffin, 1996). Little attention has been paid to the Mesozoic lithospheric boundary between the Yangtze and Cathaysia blocks.

The Yangtze and Cathaysia blocks have distinctive crustal ages and tectonic histories (HBGMR, 1988; JBMGR, 1989). Therefore, they should have different lithospheric mantle sources that could be traced by magmatism. Recent elemental and isotopic studies have focused mostly on the Mesozoic granitic magmatism in the SCB and the Cenozoic basalts distributed along the coastal provinces (Basu et al., 1991; Tu et al., 1992; Fan and Menzies, 1994; Chung et al., 1995; Li, 2000; Zou et al., 2000). These data provided important constraints concerning the Mesozoic lithosphere. However, the nature of the Mesozoic lithosphere in the SCB remains poorly understood due to the lack of systematic and comparative studies of Mesozoic mafic magmatism (Li et al., 1997, 2003; Zhao et al., 1998; Chen et al., 1999; Wang et al., 2002, 2003).

We conducted a set of geochronological and geochemical analyses of basaltic lavas and related mafic dikes around the Chenzhou-Linwu fault in order to advance our understanding of the Mesozoic lithosphere of the SCB. This made it possible to further define the lithospheric boundary between the Yangtze and Cathaysia blocks.

Geological Setting and Petrography

The Yangtze and Cathaysian blocks were consolidated by the Jinning orogenic event at ca. 970 Ma (Li and McCulloch, 1996). The basement rocks of the Yangtze block are >3.2 Ga, with an average age of 2.7–2.8 Ga (Qiu et al., 2000). In contrast, the basement of the Cathaysia block exhibits Paleo- to Mesoproterozoic and possibly late Archean ages of ~2.5 Ga (HBGMR, 1988; JBGMR, 1989; Chen and Jahn, 1998). Both basement blocks are overlain by Paleozoic continental to neritic marine sediments, and continental redbeds and volcanic-sedimentary sequences Late Triassic time onward. The entire sequence is intruded by voluminous granite plutons.

Mesozoic mafic rocks in the SCB interior occur sporadically around the Chenzhou-Linwu fault zone (Fig. 1). These mafic rocks mainly include the basaltic lavas and related mafic dikes at locations 1 to 3, to the west of the Chenzhou-Linwu fault in Hunan Province (Group 1), and those at locations 4 to 6, to the east of the Chenzhou-Linwu fault in southwestern Jiangxi Province (Group 2). To the south, the mafic rocks also crop out in southeastern Guangxi (location 7) (Li et al., 2003) and northern Guangdong provinces (Li et al., 1997).

Group 1 mafic rocks are commonly of small volume and occur as cones, pipes, sills, and dikes. The mafic dikes at locations 1 (e.g. Jiaoxiling) and 3 (Zhicun and Huilongyu) intrude the Pre-Mesozoic strata. The basalts at locations 1 (Chunhuashan) and 2 (Chunjiangpu) are conformably interbedded with Cretaceous strata, whereas those at location 3 (Ningyuan and Daoxian) unconformably overlie Upper Paleozoic sequences (D-T_2). Group 2 mafic rocks are relatively voluminous, and occur as volcanic cones (Lousishan at location 4), pipes (Changchengling at location 6), and volcanic basins (Changpu-Baimianshan, Dongkeng-Linjiang at location 5, and Rucheng at location 6) as well as minor dikes intruding Paleozoic strata.

Mesozoic mafic lithologies include basalt, trachybasalt, basaltic trachyandesite, basaltic andesite, and mafic dikes. The basaltic lavas are commonly subaphyric to porphyritic with predominant phenocrysts of olivine and/or clinopyroxene up to 0.5–2 mm. Plagioclase phenocrysts are rare. The matrix is mainly composed of fine-grained or aphanitic clinopyroxene, plagioclase, and a few opaque oxides. Mafic dikes (e.g. lamprophyre) are typically fresh, porphyritic with phenocrysts of biotite, pyroxene, and/or olivine.

Sampling and Analytical Techniques

Representative fresh samples were collected from Mesozoic basaltic lavas and mafic dikes around the Chenzhou-Linwu fault (Fig. 1). Some data published by Li et al. (1997, 2003) were selected from mafic veins in Zhouguangshan, and from basalts in southern Hunan Province.

K-Ar dating was performed employing an MM-1200 mass spectrometer at the Guangzhou Institute of Geochemistry, Chinese Academy of Science (CAS). The results, with analytical errors less than 5%, are synthesized in Table 1 and Figure 1.

Major-element abundances were obtained on a wavelength X-ray fluorescence spectrometry at the Hubei Institute of Geology and Mineral Resource, Chinese Ministry of Land and Resource, with analytical errors less than 2%. FeO content was analyzed solely by a chemical method. Trace-element analysis was performed at the Guangzhou Institute of Geochemistry, CAS by inductively coupled plasma mass spectrometry (ICP-MS). The details of the method and analytical procedure can be found in Liu et al. (1996). Major and trace elements are listed in Table 2.

Sr and Nd isotopic ratios were measured by a VG354 mass-spectrometer at the Institute of Geology and Geophysics, CAS. Sr and Nd isotopic ratios were normalized to $^{86}Sr/^{88}Sr = 0.1194$ and $^{146}Nd/^{144}Nd = 0.7219$. Measured values for NBS 987 Sr standard and La Jolla Nd standard were 0.710265 ± 12 for $^{87}Sr/^{86}Sr$ and 0.511862 ± 10 for $^{143}Nd/^{144}Nd$. The whole procedure blanks are lower than 2 to 5 × 10^{-10}g for Sr content and 5×10^{-11}g for Nd content. $^{87}Rb/^{86}Sr$ and $^{147}Sm/^{144}Nd$ ratios were calculated using the Rb, Sr, Sm, and Nd abundances measured by ICP-MS. $^{143}Nd/^{144}Nd$ and $^{147}Sm/^{144}Nd$ ratios of CHUR at the present time are 0.512638 and 0.1967, respectively. Sr-Nd isotopic ratios are listed in Table 3.

TABLE 1. Summary of Geochronology for Typical Mesozoic Mafic Rocks in the SCB[1]

Group	Method	Age, Ma	Location	Lithology	Sample	Reference
			West of Chenzhou-Linwu fault (Group 1)			
Group 1A	^{40}Ar-^{39}Ar	173.8±0.9	Ningyuan, location 3	Basalt	PA-03	Li et al., 2003
	^{40}Ar-^{39}Ar	171.8±0.8	Ningyuan, location 3	Basalt	XPA-1	Li et al., 2003
	^{40}Ar-^{39}Ar	170.3±0.9	Ningyuan, location 3	Basalt	XTB-3	Li et al., 2003
	K-Ar	169.1±2.7	Huilongyu, location 3	Mafic dike	JYH-4	This study
	K-Ar	172.2±2.7	Huilongyu, location 3	Biotite	JYH-2*	This study
Group 1B	^{40}Ar-^{39}Ar	151.6±1.0	Daoxian, location 3	Basalt	HTY-1	Li et al., 2003
	^{40}Ar-^{39}Ar	147.3±0.3	Daoxian, location 3	Basalt	DXB-1	Li et al., 2003
	K-Ar	146.2±2.3	Zhicun, location 3	Mafic dike	ZHC-10	This study
Group 1C	K-Ar	93.4±1.5	Jiaoxiling, location 1	Mafic dike	20LY-53	This study
	K-Ar	83.3±1.0	Chunhuashan, location 1	Basalt	20LY-26	This study
	K-Ar	83.1±1.3	Jiaoxiling, location 1	Mafic dike	20LY-48	This study
	K-Ar	81	Chunjiangpu, location 2	Basalt	CJP-1	Zhao et al., 1998
			East of Chenzhou-Linwu fault (Group 2)			
Group 2A	K-Ar	172.7±3.3	Baimianshan, location 6	Basalt	20GN-72	This study
	Rb-Sr	173±5.5	Baimianshan, location 6	Basalt		Chen et al., 1998
	Rb-Sr	178±7.2	Dongkeng, location 6	Basalt		Chen et al., 1998
	^{40}Ar-^{39}Ar	178.0±3.6	Changchenglin, location 5	Basalt	YTK-1	Zhao et al., 1998
Group 2B	K-Ar	139.0±2.8	Zhuguangshan,	Mafic dike	BD-29**	Li et al., 1997
	K-Ar	142.6±2.8	Zhuguangshan	Mafic dike	BD-24**	Li et al., 1997
	K-Ar	127.6±1.9	Hengshan, location 5	Basalt	20YZH-20	This study
	K-Ar	124.5±2.5	Hengshan, location 5	Basalt	20YZH-26	This study
Group 2C	^{40}Ar-^{39}Ar	90.2±0.3	Lousishan, location 4	Basalt	20JF-162	This study

[1] * = K-Ar age for biotite concentrates from lamprophyric vein; ** = K-Ar age for hornblendes from mafic dike.

Geochronology

Mafic rocks in Group 1

The lamprophyre (JYH-4) and the biotites from lamprophyre (JYH-2) in Huilongyu (location 3) yielded K-Ar ages of 172.2 and 169.1 Ma, respectively. Similar $^{40}Ar/^{39}Ar$ ages of 170–174 Ma were obtained for the basalts from Ningyuan (location 3) (Li et al., 2003; Zhao et al., 1998). A mafic dike sample (ZHC-10) from Zhicun and two basalts at Daoxian (location 3), respectively, yielded K-Ar ages of 146.2 Ma and $^{40}Ar/^{39}Ar$ plateau ages of 150–154 Ma (Li et al., 2003). K-Ar ages of 83.8 Ma for a basalt from Cretaceous strata in Chunhuashan (20LY-26 in location 1), and 83.1 Ma and 93.4 Ma for two mafic dikes intruding into pre-Sinian sequence (20LY-48 and 20LY-53 in location 1) were given, respectively, similar to that of the tholeiite from Chunjiangpu (81 Ma, location 2) (Zhao et al., 1998). Thus there are at least three main episodes of mafic extrusion on west of the Chenzhou-Linwu fault, roughly corresponding to ca. 175 Ma (Group 1A), ca. 140–152 Ma (Group 1B), and ca. 80–95 Ma (Group 1C).

Mafic rocks in Group 2

Similarly, three episodes of mafic magmatism were identified on the east of the Chenzhou-Linwu

TABLE 2. Major- and Trace-Element Analyses for Mesozoic Mafic Rocks in the SCB Interior[1]

Sample	20LY-23	20LY-24	20LY-25	20LY-26	20LY-29	20LY-30	20LY-31	20LY-32	20LY-40	20LY-42	20LY-46	20LY-48	20LY-49	20LY-51	20LY-52	20LY-55	20LY-56	20LY-57	Bao-1	HNT-100	DXB-1*	HTY-1*
	Group 1C																		Group 1B			
	80 Ma, basalt, Chunjiangpu in location 1								81Ma, basalt, in location 2		83–93 Ma, lamprophyre, Jiaoxiling area in location 1								150–154 Ma, basalt Ningyuan in location 3			
SiO_2	49.84	50.13	50.63	49.61	49.98	49.20	50.67	49.50	53.01	53.64	47.99	47.28	47.49	44.92	45.47	48.26	48.66	48.97	45.04	43.02	48.99	46.39
Al_2O_3	15.22	14.51	14.88	14.85	14.84	14.83	15.64	14.97	14.01	14.45	14.42	14.56	14.5	13.08	13.36	14.41	14.58	14.44	15.45	13.16	11.27	9.03
Fe_2O_3	5.01	4.32	4.29	4.61	4.77	5.52	4.71	5.13	2.03	2.42	4.95	4.78	5.46	5.12	4.96	3.61	3.34	3.18	5.42	2.22	8.11	6.93
FeO	5.30	6.87	5.30	5.77	5.03	5.13	5.03	5.30	7.27	6.77	5.30	5.33	4.93	6.87	6.77	6.00	6.77	6.37	6.76	7.10		
MgO	6.90	6.62	6.43	7.21	7.17	7.2	5.86	7.28	5.86	5.46	5.24	5.17	5.13	7.44	7.31	6.53	6.50	6.75	6.76	15.15	16.24	16.16
CaO	8.98	9.27	9.75	9.44	9.73	9.23	9.35	9.14	7.07	6.82	7.60	7.54	6.91	7.86	7.46	6.78	6.05	6.59	8.67	3.90	8.23	13.77
Na_2O	2.70	2.67	2.87	2.59	2.5	2.69	3.08	2.66	3.64	3.84	4.14	4.22	4.42	4.35	3.74	3.48	3.20	3.43	2.93	1.86	1.52	0.80
K_2O	0.90	0.72	1.18	0.74	0.83	0.86	1.14	0.85	1.33	1.32	2.61	2.58	2.28	1.38	2.39	3.01	3.17	2.88	1.05	1.54	3.35	2.19
MnO	0.18	0.17	0.18	0.14	0.17	0.18	0.19	0.17	0.13	0.13	0.18	0.18	0.16	0.16	0.15	0.17	0.36	0.14	0.43	0.24	0.16	0.16
TiO_2	1.87	1.80	1.98	1.92	1.90	1.95	2.06	1.91	2.08	1.93	2.16	2.11	2.18	3.35	3.32	2.42	2.37	2.21	2.36	1.46	0.67	0.56
P_2O_5	0.33	0.30	0.37	0.34	0.34	0.34	0.37	0.35	0.37	0.37	0.59	0.59	0.58	1.03	1.03	0.67	0.67	0.59	0.62	0.65	0.47	0.61
LOI	2.53	2.38	1.90	2.55	2.49	2.63	1.64	2.49	2.98	2.61	4.52	5.35	5.58	4.15	3.71	4.39	4.03	4.20	4.23	7.69		
$Mg^{\#}$	0.56	0.53	0.56	0.57	0.58	0.56	0.53	0.57	0.54	0.52	0.49	0.49	0.48	0.54	0.54	0.56	0.54	0.57	0.51	0.75	0.80	0.82
Sc	22.42	23.46	24.39	24.09	21.91	22.33	24.20	23.34	16.24	15.35	15.38	13.78	14.09	13.54	13.57	14.18	14.32	15.48	23.82	15.40		
V	194	197	207	199	195	203	215	201	138	132	178	163	173	229	214	154	159	159	212	133	208	182
Cr	230	246	246	234	218	220	233	223	174	161	67.6	60.8	71.1	110.6	97.4	132	139	152	200	294	1200	970
Co	43.1	51.0	61.0	51.7	50.9	62.7	49.9	51.9	37.1	34.6	38.9	35.0	35.5	44.4	40.2	37.4	40.5	40.7	54.0	38.7	57.7	53.0
Ni	156	160	153	152	140	142	146	142	91.9	83.7	64.5	62.2	62.3	97.6	89.2	96.5	100	106	168	265	503	619
Rb	10.82	41.48	21.12	10.03	9.82	11.33	16.07	10.29	40.79	38.79	82.71	76.79	70.83	29.77	47.03	92.61	103.8	98.52	21.31	40.17	89.00	95.00
Sr	418	474	493	475	426	457	482	453	448	465	894	852	855	766	885	594	701	617	783	360	772	1282
Y	25.09	24.24	25.31	23.83	23.49	24.84	25.99	25.00	24.06	27.88	30.17	29.12	29.18	27.36	27.69	22.87	23.26	23.39	31.92	26.67	24.20	24.50
Ce/Pb	18.66	21.61	20.11	27.93	24.30	25.61	25.48	20.17	19.02	23.80	25.24	24.16	23.15	23.60	26.15	27.68	25.89	24.56	13.06	14.21	6.22	7.55

Table continues

TABLE 2. *Continued*

Sample	20LY-23	20LY-24	20LY-25	20LY-26	20LY-29	20LY-30	20LY-31	20LY-32	20LY-40	20LY-42	20LY-46	20LY-48	20LY-49	20LY-51	20LY-52	20LY-55	20LY-56	20LY-57	Bao-1	HNT-100	DXB-1*	HTY-1*
Zr	145	139	166	151	148	154	161	153	154	148	345	330	332	354	360	222	227	212	277	281	104	104
Nb	24.55	22.64	29.44	26.08	24.98	27.12	29.52	27.32	27.15	26.74	76.81	73.94	74.57	84.90	87.09	54.61	56.05	49.43	68.20	59.10	20.10	21.30
Ba	306	422	298	341	303	327	356	323	358	363	686	636	1343	453	522	581	626	582	729	363	1326	2639
La	20.44	18.41	23.79	21.04	19.90	20.51	22.35	21.10	17.88	19.75	54.05	51.79	52.71	54.37	55.59	32.84	33.82	30.46	42.67	39.62	31.00	40.80
Ce	42.72	39.27	48.70	44.46	42.40	44.19	46.51	44.43	38.66	41.24	103.4	99.36	101.2	115.1	118.7	68.26	71.43	64.56	82.82	77.75	69.40	94.0
Pr	5.04	4.73	5.87	5.28	5.18	5.23	5.60	5.32	4.93	5.07	11.34	11.04	11.00	13.63	14.05	8.13	8.57	7.82	9.07	8.46	10.00	12.60
Nd	21.49	20.64	24.46	23.29	22.43	23.35	24.87	23.26	21.46	22.67	44.09	42.31	42.92	58.30	58.93	35.62	36.75	33.30	36.75	34.35	34.50	48.20
Sm	5.61	5.54	6.06	5.72	5.53	6.18	6.25	5.66	5.54	6.10	9.01	8.51	9.32	12.18	12.73	7.85	8.29	7.79	7.81	7.17	7.96	9.90
Eu	1.89	1.67	2.52	2.00	1.71	1.94	2.01	1.88	1.95	2.14	2.98	2.76	2.91	3.98	3.75	2.53	2.67	2.51	2.53	2.32	2.07	2.43
Gd	4.93	4.79	5.52	5.42	4.87	5.22	5.26	4.94	5.53	5.70	7.33	7.04	7.16	8.88	9.70	6.28	6.79	6.43	7.12	6.09	7.19	9.04
Tb	0.85	0.88	0.91	0.89	0.86	0.89	0.99	0.96	0.93	1.02	1.19	1.08	1.10	1.36	1.35	0.97	1.10	1.02	1.05	0.90	0.95	1.12
Dy	5.26	5.17	5.23	5.23	4.92	5.58	5.48	5.34	5.60	5.76	6.84	6.30	6.39	7.03	7.01	5.34	5.31	5.47	5.73	4.90	4.60	5.09
Ho	0.91	0.93	0.98	0.97	0.92	1.01	1.00	0.95	0.92	1.06	1.14	1.10	1.13	0.99	1.09	0.87	0.87	0.88	1.06	0.91	0.79	0.83
Er	2.62	2.44	2.57	2.44	2.50	2.45	2.99	2.43	2.38	2.57	3.05	2.87	2.92	2.35	2.61	1.97	2.18	2.31	2.89	2.51	2.07	2.05
Tm	0.36	0.35	0.36	0.34	0.32	0.31	0.35	0.37	0.30	0.36	0.42	0.39	0.36	0.30	0.31	0.27	0.27	0.29	0.39	0.34	0.29	0.27
Yb	2.03	2.17	2.21	1.99	1.91	2.25	2.32	2.26	1.95	2.03	2.63	2.39	2.51	1.72	1.70	1.44	1.45	1.70	2.44	2.13	1.73	1.58
Lu	0.29	0.28	0.31	0.27	0.26	0.31	0.31	0.31	0.24	0.25	0.34	0.32	0.32	0.20	0.20	0.19	0.20	0.19	0.36	0.31	0.25	0.23
Hf	4.55	4.15	4.76	4.74	4.61	4.98	5.23	4.68	5.12	4.98	9.90	8.70	9.10	9.73	10.02	6.39	7.08	6.14	6.66	6.97	2.52	2.42
Ta	1.44	1.44	1.75	1.64	1.45	1.61	1.75	1.58	1.56	1.54	4.71	4.44	4.52	4.89	4.83	2.96	3.12	2.74	4.29	3.81	0.55	0.53
Pb	2.29	1.82	2.42	1.59	1.75	1.73	1.83	2.20	2.03	1.73	4.10	4.11	4.37	4.88	4.54	2.46	2.76	2.63	6.30	5.50		
Th	3.64	3.31	3.70	3.59	3.48	3.52	3.79	3.52	3.46	3.52	7.83	7.67	7.78	6.43	6.52	4.28	4.63	4.49	6.78	5.86	10.10	10.20
U	0.85	0.73	1.01	0.78	0.81	0.73	0.85	0.97	0.80	0.80	2.06	1.96	1.90	1.59	1.54	1.05	1.11	1.12	1.96	1.63	3.76	3.97
Nb/U	29.02	30.85	29.30	33.65	30.88	37.10	34.65	28.13	34.03	33.55	37.32	37.71	39.17	53.50	56.59	52.01	50.36	43.98	34.74	24.06	16.08	17.08

Table continues

TABLE 2. *Continued*

Sample	ZCH-2	ZHC-4	ZHC-8	ZHC-9	ZHC-10	ZHC-12	ZHC-13	JYH-1	JYH-2	JYH-3	JYH-4	JYH-5	JYH-6	XPA-1*	PA-01*	XTB-2*	01JF-73	01JF-74	01JF-76	01JF-79	01JF-161	01JF-163	01JF-166
	Group 1B							Group 1A									Group 2C						
	146 Ma, mafic dike, Zhicun in Location 3,							172 Ma, lamprophyre, Huilongyu in Location 3,						175 Ma, basalt, Ningyuan in location,			Possibly 90 Ma, basalt, Lousishan area in location 4						
SiO_2	48.66	52.73	48.85	48.3	49.83	49.65	47.92	50.38	52.55	52.38	53.13	52.69	51.23	49.64	44.81	44.60	52.17	52.72	52.6	52.22	45.95	46.11	46.15
Al_2O_3	9.28	12.71	9.55	8.92	9.38	9.37	9.08	11.98	12.48	12.54	12.64	12.56	11.13	16.15	14.77	14.76	16.06	16.46	16.2	16.75	15.08	15.31	14.95
Fe_2O_3	1.51	3.00	2.80	2.40	3.02	2.75	5.60	3.22	3.27	3.19	3.44	3.46	3.44	10.82	12.65	12.53	3.38	3.20	2.57	3.66	3.20	3.57	3.05
FeO	6.27	3.67	4.87	5.37	4.70	4.93	4.90	3.93	3.50	3.60	3.30	3.27	4.20					5.23	5.97	4.57	7.75	7.12	7.68
MgO	17.58	6.64	15.86	17.91	15.13	15.04	15.24	7.91	6.92	6.98	6.73	6.85	8.30	6.62	8.23	8.17	6.55	5.99	6.34	6.16	7.93	7.52	7.58
CaO	6.86	9.58	6.92	6.38	6.94	6.97	6.65	10.83	10.19	10.04	9.56	9.93	11.63	6.63	10.18	10.28	8.92	8.98	8.81	9.50	9.23	8.90	8.76
Na_2O	1.34	2.43	1.16	1.27	1.09	1.06	1.00	2.24	2.49	2.38	2.36	2.45	1.87	3.81	3.19	3.25	2.91	2.96	2.98	2.86	4.26	4.19	4.22
K_2O	4.28	4.04	3.72	3.92	4.2	3.96	4.17	3.54	3.81	3.87	3.94	3.86	3.52	2.16	0.66	0.76	0.63	1.03	1.02	0.68	0.55	0.82	0.67
MnO	0.15	0.18	0.15	0.15	0.14	0.16	0.15	0.13	0.15	0.17	0.17	0.14	0.18	0.19	0.19	0.19	0.16	0.14	0.16	0.11	0.16	0.17	0.17
TiO_2	0.56	0.64	0.57	0.57	0.58	0.59	0.56	0.79	0.70	0.76	0.76	0.77	0.75	1.79	2.68	2.67	1.14	1.17	1.13	1.17	2.79	2.70	2.71
P_2O_5	0.54	0.55	0.54	0.53	0.56	0.56	0.53	0.55	0.57	0.57	0.55	0.56	0.53	0.76	0.66	0.66	0.23	0.27	0.27	0.28	0.82	0.81	0.82
LOI	2.51	3.30	4.54	3.80	3.98	4.56	3.75	4.02	2.95	3.15	3.01	3.07	3.00				1.83	1.64	1.75	1.87	1.96	2.46	2.90
$Mg^{\#}$	0.81	0.66	0.79	0.81	0.79	0.79	0.73	0.68	0.66	0.66	0.65	0.66	0.67	0.55	0.57	0.54	0.57	0.57	0.58	0.59	0.57	0.57	0.57
Sc	22.04	19.08	22.18	21.97	22.09	22.24	21.80	19.09	17.73	19.60	17.99	18.59	19.74				19.73	20.27	21.48	21.66	21.96	21.99	22.03
V	136	151	135	132	137	134	137	156	151	158	152	152	145	140	274	273	197	193	219	234	240	239	233
Cr	1290	201	1341	1478	1374	1338	1320	360	248	744	253	236	650	204	216	273	178	190	141	205	188	153	336
Co	60.1	27.5	59.2	57.5	58.1	58.8	57.4	34.5	28.0	30.8	30.6	28.6	37.9	32.9	50.2	49.7	56.0	49.2	41.2	36.5	43.1	41.1	42.5
Ni	647	123	621	634	631	611	614	240	147	390	151	140	378	149	149	149	163	140	98.5	101	138	116	205
Rb	145.8	205.1	125.5	129.4	135.1	132.8	151.1	333	434	437	345	449	293	47.10	11.00	7.10	14.38	18.86	20.05	6.64	32.32	49.41	38.67
Sr	674	578	551	485	531	459	567	727	658	655	638	668	560	743	971	985	361	387	366	416	905	1064	1009
Y	18.09	21.28	18.10	17.81	18.57	17.11	18.02	21.93	21.91	22.67	24.77	22.31	20.26	30.50	30.20	29.80	18.08	25.87	17.01	18.20	27.06	25.77	26.90

Table continues

TABLE 2. *Continued*

	ZCH-2	ZHC-4	ZHC-8	ZHC-9	ZHC-10	ZHC-12	ZHC-13	JYH-1	JYH-2	JYH-3	JYH-4	JYH-5	JYH-6	XPA-1*	PA-01*	XTB-2*	01JF-73	01JF-74	01JF-76	01JF-79	01JF-161	01JF-163	01JF-166
Zr	111	159	116	108	115	104	114	140	146	153	160	152	118	354	267	258	90	98	95	101	225	227	230
Nb	12.96	34.29	13.35	12.37	13.58	12.08	13.14	30.73	32.97	33.99	35.98	34.19	27.59	78.90	67.30	67.00	18.23	21.23	20.28	21.94	67.96	69.00	71.47
Ba	1184	1759	1493	1250	1518	1095	1359	2240	1739	1681	1843	1816	1646	537	483	517	253	292	287	302	666	680	716
La	23.52	41.01	23.75	23.05	24.02	22.91	24.05	39.46	42.91	43.39	46.44	44.49	40.52	48.40	39.60	39.50	14.69	17.34	16.83	17.57	43.40	43.50	44.84
Ce	47.71	76.48	47.25	46.19	48.29	46.74	48.11	73.68	78.87	77.20	75.50	81.27	72.77	95.10	78.20	77.70	29.80	34.53	32.56	34.90	85.91	86.45	88.34
Pr	5.71	8.62	5.71	5.40	5.78	5.45	5.74	8.79	9.31	9.37	9.21	9.40	8.28	11.30	9.50	9.50	3.35	3.81	3.82	3.84	9.24	9.48	9.75
Nd	23.08	33.88	23.12	23.49	23.82	22.39	23.41	34.14	36.29	36.84	38.81	37.42	32.35	43.20	37.60	37.70	13.45	15.62	14.72	16.18	38.06	38.55	38.81
Sm	4.43	6.83	4.61	4.34	4.79	4.66	4.62	6.32	7.20	7.12	7.26	6.95	5.99	8.23	7.32	7.70	3.00	3.64	3.51	3.68	7.58	7.74	8.08
Eu	1.14	1.57	1.10	1.02	1.16	1.02	1.13	1.74	1.82	1.83	1.86	1.74	1.61	2.62	2.49	2.43	1.11	1.30	1.16	1.26	2.53	2.47	2.49
Gd	3.84	5.61	4.13	3.87	3.87	3.89	4.03	5.61	5.92	5.91	5.98	6.00	5.30	7.27	7.19	7.26	3.40	3.87	3.42	3.72	6.92	6.93	7.37
Tb	0.58	0.74	0.59	0.56	0.56	0.53	0.58	0.77	0.80	0.80	0.79	0.81	0.68	1.04	1.06	1.05	0.63	0.67	0.59	0.63	1.05	1.05	1.12
Dy	3.48	4.15	3.36	3.33	3.46	3.30	3.32	4.14	4.32	4.37	4.38	4.26	4.13	5.61	5.63	5.58	3.38	3.96	3.40	3.56	5.15	5.17	5.77
Ho	0.70	0.76	0.67	0.63	0.62	0.63	0.65	0.80	0.82	0.83	0.81	0.84	0.71	1.02	1.03	1.02	0.70	0.77	0.70	0.69	1.02	1.01	1.01
Er	1.93	2.07	1.90	1.80	1.87	1.92	1.79	2.26	2.19	2.32	2.18	2.25	2.07	2.79	2.73	2.66	1.80	2.17	1.84	1.90	2.48	2.57	2.61
Tm	0.25	0.32	0.29	0.27	0.27	0.28	0.27	0.34	0.31	0.33	0.31	0.32	0.30	0.40	0.38	0.37	0.25	0.29	0.27	0.24	0.32	0.34	0.33
Yb	1.62	2.03	1.85	1.68	1.78	1.69	1.65	1.94	1.99	2.02	2.09	2.12	1.72	2.45	2.27	2.21	1.65	1.79	1.68	1.69	2.01	2.13	2.20
Lu	0.26	0.32	0.25	0.26	0.26	0.24	0.24	0.31	0.32	0.32	0.34	0.30	0.27	0.36	0.33	0.32	0.28	0.30	0.28	0.25	0.31	0.32	0.32
Hf	3.25	4.40	3.32	3.11	3.29	2.98	3.17	4.08	4.32	4.49	4.36	4.25	3.70	7.83	5.90	5.63	2.48	2.53	2.43	2.65	5.32	5.48	5.45
Ta	0.62	1.70	0.70	0.65	0.69	0.62	0.73	1.50	1.66	1.76	1.75	1.76	1.47	4.78	4.64	3.95	0.99	1.29	1.29	1.35	4.30	4.46	4.61
Pb	11.20	22.7	12.37	10.25	13.03	10.12	12.06	18.42	21.05	21.30	21.20	20.48	34.15				1.19	1.32	1.21	1.77	2.52	2.75	3.45
Th	4.10	12.02	4.25	4.06	4.29	3.79	4.30	10.44	11.87	12.46	12.90	11.86	9.90	7.99	6.20	6.15	3.15	3.76	3.64	3.79	5.22	5.28	5.53
U	0.88	4.00	0.86	0.77	0.89	0.74	0.87	3.39	3.75	4.01	4.14	3.78	2.98	2.45	2.01	1.99	0.64	0.74	0.74	0.77	1.28	1.26	1.33
Nb/U	14.81	14.24	15.51	16.02	15.20	16.37	15.08	9.08	8.80	8.48	8.69	9.04	9.26	32.20	33.48	33.67	41.81	48.14	45.89	46.39	53.26	54.59	53.70
Ce/Pb	4.26	3.37	3.82	4.51	3.86	4.46	4.09	4.15	3.76	3.72	3.61	4.12	2.16				25.10	26.08	26.95	19.77	34.06	31.41	25.58

Table continues

TABLE 2. *Continued*

Sample	20YZH-16	20YZH-17	20YZH-18	20YZH-21	20YZH-25	20YZH-26	20YZH-27	20GN-42	20GN-43	20GN-45	20GN-77	20GN-36	20YZH-2	20YZH-4	20YZH-5	20YZH-7	20YZH-8	20YZH-9	20YZH-10	20YZH-11	20YZH-13
	Group 2B							Group 2A													
	ca. 125 Ma, basalt, Hengshan in location 5							ca. 175 Ma, basalt, Baimianshan and Changpu in Location 6					ca. 178 Ma, basalt, Changchengling in location 5								
SiO_2	45.20	47.72	49.93	49.96	49.75	50.41	50.17	50.02	50.77	50.05	50.4	53.11	51.41	50.25	51.19	52.24	51.95	53.51	51.92	52.16	49.87
Al_2O_3	14.68	14.72	15.18	15.09	15.4	15.15	15.48	16.7	15.7	15.45	16.47	15.14	17.24	17.11	17.24	17.07	17.33	16.26	16.43	16.01	17.03
Fe_2O_3	2.37	2.37	1.04	1.20	1.19	1.28	0.68	1.63	1.86	1.90	3.55	1.62	3.32	2.93	2.80	3.30	2.97	2.17	2.32	2.20	2.56
FeO	10.01	9.44	8.47	7.57	7.55	8.10	8.73	8.03	7.92	8.70	6.15	8.08	6.11	7.13	7.02	6.73	6.74	6.28	6.62	7.13	7.40
MgO	4.94	5.21	8.67	8.37	8.52	8.11	8.12	7.65	6.59	6.65	6.74	5.79	3.95	3.84	4.21	4.18	3.94	2.92	3.44	3.18	3.24
CaO	11.25	9.61	10.11	11.44	11.23	10.37	10.37	8.55	9.44	9.81	10.65	7.52	10.13	10.98	9.68	8.92	9.40	10.79	11.21	10.93	11.33
Na_2O	2.70	3.15	1.49	1.87	1.69	1.74	1.80	2.71	2.80	2.68	1.81	2.81	2.20	2.23	1.97	2.45	2.50	2.07	1.82	1.72	1.82
K_2O	0.70	0.57	0.27	0.27	0.20	0.27	0.22	0.95	1.04	0.78	0.46	1.87	0.28	0.31	0.36	0.62	0.52	0.85	0.70	0.66	0.55
MnO	0.12	0.13	0.17	0.15	0.16	0.18	0.16	0.15	0.16	0.17	0.2	0.15	0.14	0.13	0.11	0.13	0.13	0.13	0.16	0.12	0.12
TiO_2	2.70	2.78	1.37	1.35	1.31	1.42	1.44	1.39	1.58	1.60	1.53	1.62	1.85	2.07	2.01	1.98	1.96	1.97	2.04	2.06	2.04
P_2O_5	0.51	0.57	0.15	0.15	0.15	0.16	0.16	0.23	0.27	0.25	0.18	0.3	0.28	0.32	0.30	0.30	0.29	0.30	0.31	0.33	0.32
LOI	4.42	3.45	2.99	2.56	2.72	2.62	2.48	1.98	1.69	1.77	1.70	1.80	3.00	2.61	3.00	2.05	2.24	2.61	2.85	3.32	3.53
$Mg^{\#}$	0.42	0.45	0.62	0.64	0.64	0.61	0.61	0.59	0.55	0.53	0.56	0.52	0.44	0.41	0.44	0.44	0.43	0.39	0.42	0.39	0.38
Sc	15.49	15.50	28.31	25.25	27.92	31.66	31.69	21.10	30.15	34.70	30.01	24.22	20.62	25.02	22.64	25.44	23.47	21.42	22.36	21.53	22.30
V	183	165	276	282	269	285	286	171	218	255	243	192	184	220	202	221	206	198	198	194	192
Cr	135	107	461	447	449	399	411	79.1	102.9	101.4	42.2	70.9	25.42	34.34	28.37	29.50	27.95	25.77	29.99	25.47	29.70
Co	56.2	45.2	52.7	52.5	53.2	54.7	51.5	54.8	48.3	58.2	48.3	44.8	33.2	39.7	36.3	40.3	36.5	32.6	32.5	33.2	36.3
Ni	142	108	103	99.7	100	85.6	86.4	125.7	58.5	50.8	34.7	64.9	36.9	47.3	40.1	44.8	40.2	36.0	42.3	37.5	40.1
Rb	35.45	28.92	7.62	6.53	5.66	6.74	7.60	45.28	49.42	35.85	154. 6	97.35	5.86	8.18	12.67	18.94	6.95	60.62	41.08	48.52	37.73
Sr	412	442	279	308	304	299	296	324.9	333.7	316.4	278.6	295.7	400	455	373	498	438	413	354	320	336
Y	22.90	26.14	20.40	19.82	20.63	22.98	21.19	27.79	30.39	28.69	45.36	41.84	23.60	28.10	26.09	28.31	26.12	25.60	26.14	26.88	26.16

Table continues

TABLE 2. *Continued*

	20YZH-16	20YZH-17	20YZH-18	20YZH-21	20YZH-25	20YZH-26	20YZH-27	20GN-42	20GN-43	20GN-45	20GN-77	20GN-36	20YZH-2	20YZH-4	20YZH-5	20YZH-7	20YZH-8	20YZH-9	20YZH-10	20YZH-11	20YZH-13
Zr	211	234	102	104	103	109	110	119	88.48	111.7	108.2	185.0	127	152	145	154	144	142	143	145	144
Nb	36.25	40.57	8.58	8.73	8.76	8.95	9.07	18.70	20.00	17.08	12.50	26.94	12.16	14.82	13.78	14.62	13.46	13.59	13.17	13.32	13.70
Ba	429	494	177	200	167	191	138	167.8	183.6	159.2	223.9	245.5	281	294	240	362	370	568	284	209	180
La	26.74	29.49	11.89	11.97	12.21	13.33	12.79	19.20	20.48	17.43	18.54	28.32	16.94	20.30	18.42	19.81	17.75	18.67	19.19	18.34	19.44
Ce	56.66	63.06	27.16	27.52	27.75	30.07	29.68	41.59	44.16	38.47	39.94	61.16	36.68	43.63	40.58	44.23	40.04	40.90	40.81	40.02	41.92
Pr	6.89	7.61	3.38	3.55	3.51	3.96	3.72	5.01	5.44	4.77	4.87	7.32	4.60	5.54	4.98	5.37	5.11	4.95	4.97	5.08	5.04
Nd	29.87	33.58	15.50	15.66	15.76	16.47	16.41	21.24	22.92	20.57	21.46	29.72	20.27	23.73	22.21	24.30	21.82	22.00	22.10	22.06	22.06
Sm	6.80	7.38	3.73	3.78	3.77	4.61	4.32	4.93	5.56	5.32	4.94	7.37	4.63	5.63	5.35	5.75	5.22	4.80	5.08	5.14	5.19
Eu	2.45	2.62	1.40	1.44	1.46	1.53	1.49	1.46	1.61	1.51	1.72	1.81	1.69	1.90	1.79	1.82	1.79	1.66	1.77	1.81	1.75
Gd	6.98	7.92	4.11	4.00	3.87	4.51	4.47	5.37	5.64	5.42	5.42	6.93	4.62	5.85	5.47	5.91	5.40	5.51	5.16	5.36	5.16
Tb	0.98	1.10	0.63	0.64	0.62	0.69	0.68	0.84	0.91	0.88	0.83	1.12	0.76	0.97	0.83	0.94	0.85	0.80	0.87	0.84	0.85
Dy	5.57	5.80	3.90	4.19	3.82	4.12	4.10	5.01	5.75	5.09	5.25	7.02	4.36	5.46	5.10	5.58	4.96	5.20	5.34	4.97	4.95
Ho	0.98	0.99	0.69	0.75	0.72	0.80	0.82	0.95	1.13	1.12	0.97	1.38	0.91	1.03	1.06	1.11	0.96	0.98	1.00	0.99	0.97
Er	2.37	2.59	2.30	2.14	2.11	2.39	2.31	2.94	3.19	3.08	3.17	3.97	2.48	3.06	2.95	3.10	2.81	2.86	2.83	2.91	2.84
Tm	0.28	0.29	0.30	0.33	0.28	0.34	0.34	0.39	0.43	0.41	0.37	0.52	0.36	0.41	0.39	0.44	0.39	0.38	0.42	0.36	0.34
Yb	1.64	1.87	1.99	1.84	1.96	2.08	2.01	2.54	2.97	2.67	2.40	3.77	2.25	2.71	2.62	2.86	2.53	2.54	2.50	2.77	2.49
Lu	0.18	0.22	0.30	0.30	0.27	0.28	0.31	0.34	0.41	0.40	0.33	0.54	0.32	0.40	0.39	0.41	0.44	0.38	0.42	0.36	0.36
Hf	5.75	6.18	2.85	3.31	3.28	3.36	3.55	3.39	2.74	3.36	3.20	5.88	3.66	4.57	4.14	4.64	4.23	4.20	4.32	4.47	4.14
Ta	2.43	2.60	0.58	0.59	0.61	0.59	0.62	1.23	1.34	1.15	1.77	1.72	0.68	0.86	0.79	0.87	0.83	0.76	0.80	0.82	0.75
Pb	2.86	3.60	2.05	2.09	2.32	2.98	1.57	6.01	6.44	5.64	4.46	10.29	4.64	5.64	5.11	5.91	5.02	5.69	5.07	5.02	4.90
Th	3.29	3.87	2.24	2.24	2.30	2.48	2.50	6.95	7.32	5.61	2.70	11.81	2.62	2.04	2.94	3.08	2.94	2.86	2.92	2.92	2.92
U	0.90	1.06	0.38	0.38	0.38	0.48	0.42	1.50	1.40	1.10	1.33	2.25	1.31	1.39	1.37	1.41	1.37	1.39	1.36	1.37	1.36
Nb/U	40.28	19.81	22.46	23.09	22.99	18.61	21.74	12.45	14.33	15.55	37.88	10.56	9.27	10.68	10.07	10.35	9.84	7.63	9.71	9.75	10.11
Ce/Pb	38.27	17.52	13.28	13.19	11.97	10.09	18.95	6.92	6.86	6.82	8.96	5.94	7.90	7.73	7.95	7.48	7.98	7.19	8.05	7.97	8.55

[1]Samples with asterisks are from Li et al., 2003.

TABLE 3. Sr-Nd Isotopic Analyses for Mesozoic Mafic Rocks around the Chenzhou-Linwu Fault[1]

Sample	Sm	Nd	Rb	Sr	$^{147}Sm/^{144}Nd$	$^{87}Rb/^{86}Sr$	$^{143}Nd/^{144}Nd(2\sigma)$	$^{87}Sr/^{86}Sr(2\sigma)$	$^{87}Sr/^{86}Sr(t)$	εNd(t)
						Group 1A				
XPA-1*	8.23	43.20	47.10	743	0.115	0.184	0.512846 (13)	0.703977 (14)	0.703520	5.88
PA-01*	7.32	37.60	11.00	971	0.118	0.033	0.512859 (21)	0.703986 (16)	0.703904	6.08
XTB-2*	7.70	37.70	7.10	985	0.124	0.021	0.512867 (14)	0.704076 (17)	0.704024	6.10
JYH-1	6.32	34.14	332.8	727.1	0.112	1.327	0.512474 (7)	0.707563 (19)	0.704356	–1.36
JYH-4	7.26	38.81	344.8	638.1	0.113	1.385	0.512458 (11)	0.708289 (12)	0.704942	–1.70
JYH-6	5.99	32.35	292.5	559.9	0.112	1.515	0.512476 (12)	0.708002 (18)	0.704341	–1.32
Bao-1	7.81	36.75	21.31	783.4	0.129	0.079	0.512814 (9)	0.703414 (20)	0.703167	5.35
HNT-100	7.17	34.35	40.17	359.8	0.126	0.324	0.512650 (10)	0.705259 (14)	0.704246	2.22
						Group 1B				
DXB-1*	7.96	34.50	89.00	772.0	0.140	0.334	0.512514 (16)	0.706115 (16)	0.705402	–1.33
HTY-1*	9.90	48.20	95.00	1282	0.124	0.215	0.512530 (17)	0.705865 (14)	0.705407	–0.72
ZHC-4	6.83	33.88	205.1	577.6	0.122	1.029	0.512475 (8)	0.707826 (21)	0.705338	–1.56
ZHC-8	4.61	23.12	125.5	551.3	0.120	0.660	0.512368 (8)	0.707834 (21)	0.706239	–3.61
ZHC-10	4.79	23.82	135.1	531.4	0.122	0.737	0.512372 (8)	0.707889 (18)	0.706108	–3.56
ZHC-13	4.62	23.41	151.1	567.2	0.119	0.772	0.512360 (9)	0.708817 (16)	0.706951	–3.75
						Group 1C				
20LY-24	5.54	20.64	41.48	473.5	0.149	0.061	0.512877 (12)	0.704522 (21)	0.704420	5.28
20LY-26	5.72	23.29	10.03	474.8	0.151	0.067	0.512855 (9)	0.704830 (20)	0.704735	4.81
20LY-29	5.53	22.43	9.82	426.0	0.152	0.097	0.512870 (10)	0.705016 (20)	0.704879	5.10
20LY-31	6.25	24.87	16.07	481.9	0.147	0.066	0.512880 (15)	0.704601 (18)	0.704507	5.35
20LY-46	9.01	44.09	82.71	894.2	0.124	0.268	0.512974 (13)	0.704120 (20)	0.703625	7.77
20LY-48	8.51	42.31	76.79	852.1	0.122	0.261	0.512984 (12)	0.703960 (16)	0.703477	8.00
20LY-49	9.32	42.92	70.83	855.2	0.131	0.240	0.512980 (15)	0.703978(25)	0.703534	7.76
20LY-51	12.18	58.30	29.77	766.2	0.126	0.113	0.512830 (12)	0.705374 (22)	0.705166	4.91
						Group 2A				
20YZH-2	4.63	20.27	5.86	400.0	0.138	0.042	0.512567 (18)	0.708109 (19)	0.708000	–0.04
20YZH-5	5.35	22.21	12.67	373.0	0.146	0.098	0.512629 (9)	0.708116 (26)	0.707864	1.00
20YZH-8	5.22	21.82	6.95	438.3	0.145	0.046	0.512555 (9)	0.707624 (22)	0.707506	–0.43
20YZH-10	5.08	22.10	41.08	353.8	0.139	0.337	0.512624 (8)	0.707956 (25)	0.707094	1.05
20YZH-11	5.14	22.06	48.52	320.4	0.141	0.439	0.512621 (10)	0.708725 (20)	0.707601	0.95
20YZH-13	5.19	22.06	37.73	336.1	0.142	0.325	0.512628 (11)	0.708420 (20)	0.707587	1.05
20GN-42	4.93	21.24	45.29	324.9	0.140	0.404	0.512565 (10)	0.708805 (19)	0.707800	–0.16
20GN-43	5.51	21.82	49.12	331.7	0.150	0.428	0.512476 (8)	0.709581 (22)	0.708513	–2.04
20GN-45	5.32	20.57	35.85	316.4	0.156	0.328	0.512504 (12)	0.709482 (25)	0.708665	–1.71
20GN-77	4.87	21.47	20.01	154.6	0.137	0.375	0.512511 (10)	0.708000(19)	0.707800	–1.17
20GN-36	7.37	29.72	57.35	295.69	0.150	0.562	0.512557(15)	0.707762(19)	0.706403	–0.57
						Group 2B				
20YZH-21	3.78	15.66	6.53	308.0	0.146	0.061	0.512631 (11)	0.708325 (20)	0.708168	1.03
20YZH-25	3.77	15.76	5.66	303.8	0.145	0.054	0.512621 (9)	0.708255 (20)	0.708117	0.87
20YZH-26	4.61	16.47	6.74	299.2	0.169	0.065	0.512630 (15)	0.708485 (20)	0.708318	0.48
						Group 2C				
01JF-73	3.00	13.45	14.38	361.0	0.135	0.115	0.512834 (11)	0.704226 (23)	0.704095	4.47
01JF-74	3.64	15.62	18.86	386.5	0.141	0.141	0.512814 (9)	0.704575 (18)	0.704414	3.99
01JF-76	3.51	14.72	20.05	366.2	0.144	0.159	0.512961 (14)	0.703789 (19)	0.703609	6.84
01JF-79	3.68	16.18	6.64	415.9	0.138	0.046	0.512869 (15)	0.703601 (28)	0.703548	5.11
01JF-161	7.58	38.06	32.32	905	0.121	0.104	0.512851 (15)	0.704645 (20)	0.704552	5.03
01JF-163	7.74	38.55	49.41	1064	0.121	0.135	0.512966 (14)	0.703619 (20)	0.703260	7.17

[1]Samples with asterisks were from Li et al., 2003.

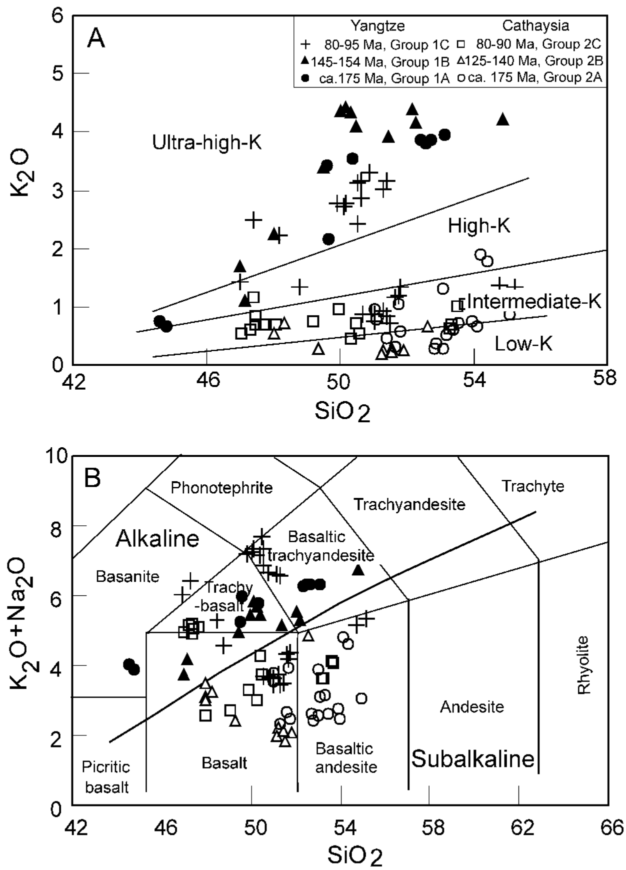

FIG. 2. SiO_2 vs. K_2O plots (A) and TAS diagrams (B); the classification scheme is after Morrison (1980) and Middlemost (1994), respectively.

fault, respectively corresponding to ca. 175 Ma (Group2A), 125–140 Ma (Group 2B), and ca. 90 Ma (Group 2C). Group 2A ages were obtained for basalts (173–178 Ma, K-Ar and Rb-Sr) from the Changpu-Beimianshan basin (location 6) (Chen et al, 1999) and Changchengling (location 5, 178 Ma $^{40}Ar/^{39}Ar$) (Zhao et al., 1998). The ages of 125–140 Ma was yielded by basalts (20YZH-20, 127.6 Ma/K-Ar, and 20YZH-26, 124.5 Ma/K-Ar) from Rucheng (location 5), and a mafic dike from Zhuguangshan (139–143 Ma, K-Ar) (Li et al., 1997). A $^{40}Ar/^{39}Ar$ plateau age of 90 Ma was obtained from a basalt in Lousishan (location 4) that is conformably interlayered in the lower part of Upper Cretaceous strata. The geochronology for Groups 1 and 2 mafic rocks in the SCB is summarized in Table 1.

Geochemical Characteristics

Major elements

Group 1 rocks with ages of >125 Ma (Groups 1A and 1B) show high K_2O and K_2O+Na_2O. They plot in the ultrahigh-K series in an SiO_2-K_2O diagram, and in the alkaline basanite, basalt, trachybasalt, and basaltic trachyandesite in a TAS diagram (Fig. 2). Samples with ages of 80–95 Ma (Group 1C) have variable K_2O contents and fall within the intermediate- to ultra-K calc-alkaline field. In contrast, Group 2 rocks are commonly characterized by low- to intermediate-K series and are classified as subalkaline basalt and basaltic andesite.

Samples from both groups exhibit a wide range of $Mg^{\#}$ (0.30–0.80). Group 1 samples generally have

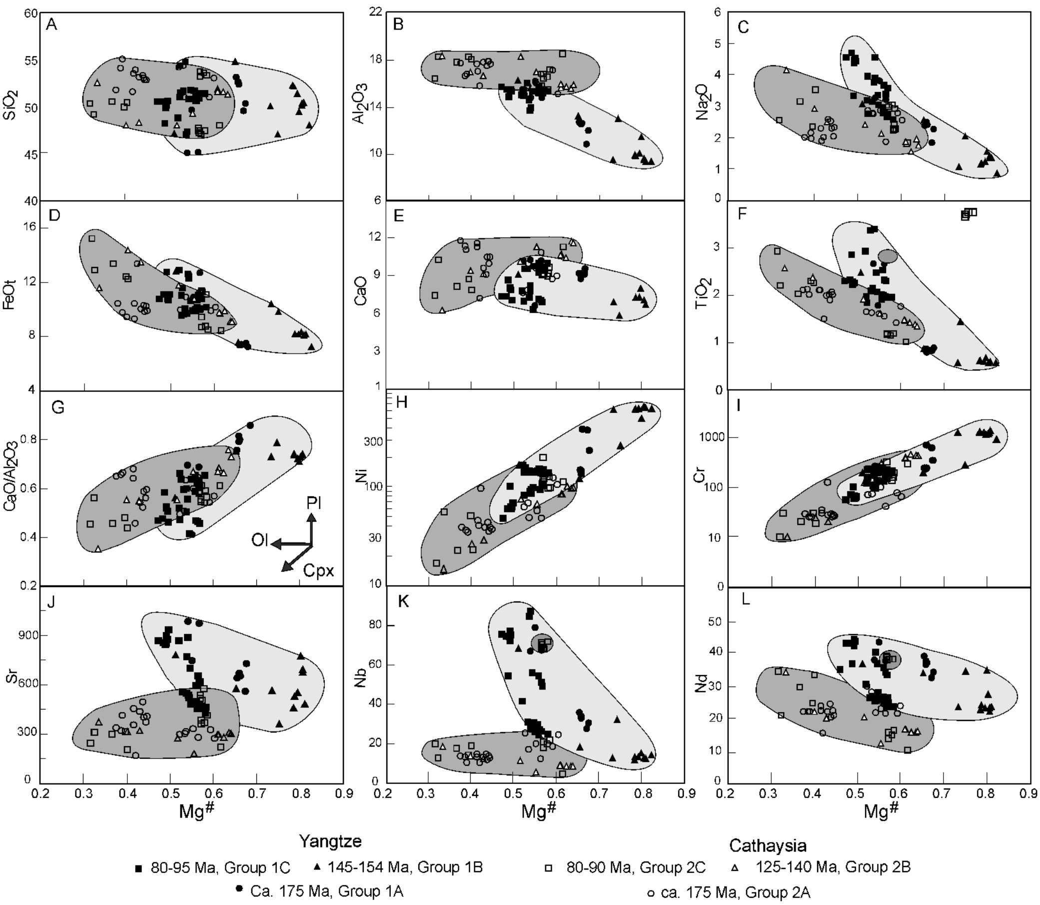

FIG. 3. Variation of major and trace elements against $Mg^{\#}$ for Mesozoic mafic rocks in the SCB interior. The symbols in (A) also apply for (B–L).

higher $Mg^{\#}$ than those of Group 2, and all high-$Mg^{\#}$ samples, with $Mg^{\#} > 65$, belong to Groups 1A and 1B. SiO_2 contents show irregular variations with increasing $Mg^{\#}$. Group 1 samples generally exhibit higher K_2O, P_2O_5, Ni, Cr, and Sr contents and lower Al_2O_3 than those in Group 2 (Table 2, Fig. 3). The distinct slope between groups, observed in oxide%–$Mg^{\#}$ and Ni-, Cr-, CaO/Al_2O_3–$Mg^{\#}$ diagrams, indicates that fractionation of pyroxene and Ti-Fe oxides, and olivine fractionation/accumulation were involved in the genesis of these rocks (Fig. 3). The geochemical contrasts between groups suggest that they probably originated from two different magmatic systems.

Incompatible elements

Basaltic rocks in the SCB interior show a wide range of trace-element contents (Table 2). Group 1 samples generally exhibit higher trace-element concentrations, especially incompatible-element contents (e.g., Rb, Ba, Sr, Nb, La, Nd) in comparison with Group 2 samples. In $Mg^{\#}$-element diagrams (Fig. 3), these two groups plot along different linear trends.

Chondrite-normalized REE patterns are shown in Figure 4. All samples show significant LREE enrichment and slightly HREE fractionation, with no evident Eu anomalies (0.75–1.13). Group 1A and 1B samples have higher $(La/Yb)_{cn}$ (9.1–21.1) but similar $(Gd/Yb)_{cn}$ (1.6–2.9) to Group 2A and 2B ($(La/Yb)_{cn}$ = 2.5–6.9, $(Gd/Yb)_{cn}$ = 1.6–2.5). However, Groups 1C and 2C show a variable LREE-enriched REE pattern with $(La/Yb)_{cn}$ = 6.1–16.4, $(Gd/Yb)_{cn}$ = 1.8–3.9, and inappreciable Eu anomalies (0.93–1.13).

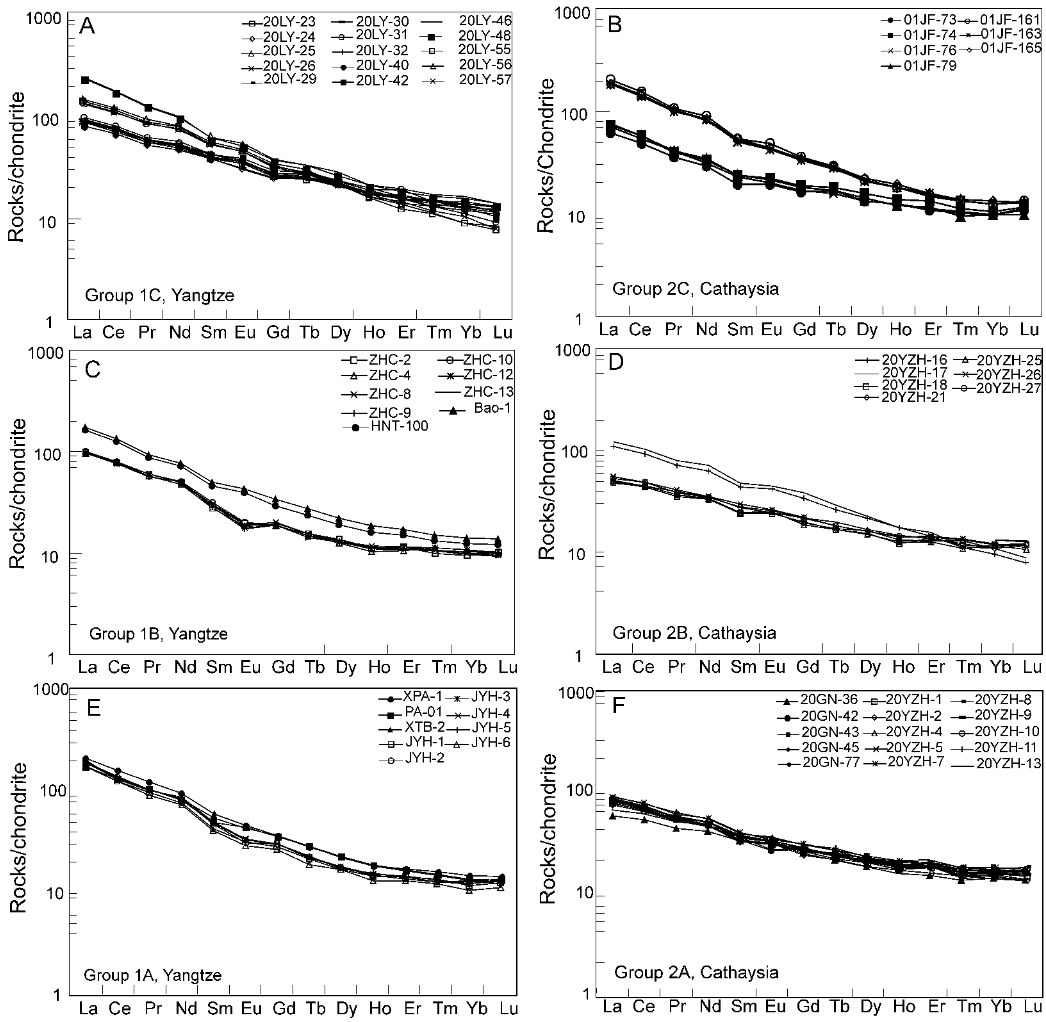

FIG. 4. Chondrite-normalized REE patterns (A–F) for Mesozoic mafic rocks of the Yangtze and Cathaysia blocks. Normalized values for chondrite are from Taylor and McLennan (1985).

In primitive-mantle normalized spidergrams (Fig. 5), high-Mg# rocks show "spiky" patterns with evident negative Nb-Ta-Ti anomalies, a positive Pb anomaly, and significant enrichment in Rb, Ba, and LREE. These anomalies are indicative of island arc–related volcanics and continental crustal rocks. In contrast, low-Mg# basaltic rocks from both groups consistently have "humped" patterns with variable enrichment of Nb-Ta, similar to those in continental rifts and ocean islands lacking appreciable crustal contamination (Hofmann, 1986; Sun and McDonough, 1989; Zou et al., 2000).

Sr-Nd isotopic ratios

Measured and age-corrected $^{87}Sr/^{86}Sr$ and $^{143}Nd/^{144}Nd$ ratios are listed in Table 3. Samples from Groups 1C and 2C have a similar range of Sr-Nd isotopic compositions ($\varepsilon_{Nd(t)}$ = +3.99 to + 8.00 and $^{87}Sr/^{86}Sr(t)$ = 0.7033–0.7052). However, Group 1B rocks show higher $^{87}Sr/^{86}Sr(t)$ (0.7032–0.7062), and a larger range of εNd(t) (-3.75 to + 5.35) than Group 2B ($^{87}Sr/^{86}Sr(t)$ = 0.7053–0.7083 and $\varepsilon_{Nd(t)}$ = +0.48 to + 4.93). Group 1A samples display two different ranges of isotopic compositions. High-Mg# samples with arc-island-

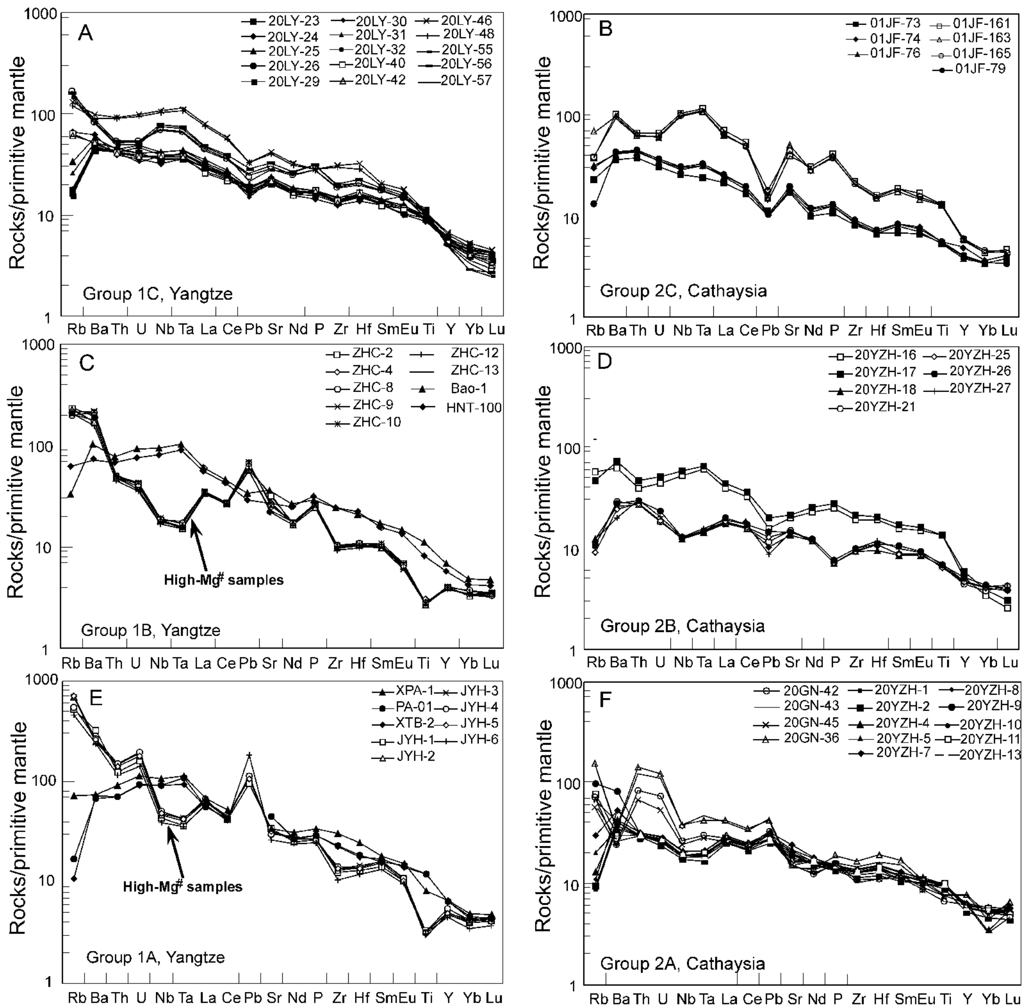

FIG. 5. Primitive mantle-normalized spidergrams (A–F) for Mesozoic mafic rocks of the Yangtze and Cathaysia blocks. Normalized values for primitive mantle are from Sun and McDonough (1989).

like trace-element patterns have $^{87}Sr/^{86}Sr(t)$ = 0.7043–0.7049 and $\varepsilon_{Nd(t)}$ = –1.32 to –1.70, and low-Mg# samples with OIB-like trace element patterns have $^{87}Sr/^{86}Sr(t)$ = 0.7035–0.7040 and $\varepsilon_{Nd(t)}$ = +4.64 to +5.05. In contrast, Group 2A samples exhibit $^{87}Sr/^{86}Sr(t)$ ratios of 0.7061–0.7087 and $\varepsilon_{Nd(t)}$ values of –2.04 to +1.05.

On a $^{87}Sr/^{86}Sr(t)$ vs. $\varepsilon_{Nd(t)}$ diagram (Fig. 6), Group 1 samples define a mantle array that is constituted by Hawaii-OIB basalt and Kenya–Patagonia–Walvis Ridge–Kerguelen–Northern Karoo basalts with an EMI-type source. Group 2 samples lie along the other mantle array between the Hawaii-OIB field and EMII-type source characterized by Samoa–Society islands–Afar–Etendeka (Hawkesworth et al., 1984). In general Group 1A and 1B have low $^{87}Sr/^{86}Sr(t)$ ratios, a remarkably narrow $^{87}Sr/^{86}Sr(t)$ range, but a large Nd isotopic composition range, in comparison with those in Groups 2A and 2B.

Discussion

Low-temperature alteration and crustal contamination

Before speculating on their mantle sources, it is important to assess whether or not the samples have undergone low- temperature alteration and crustal

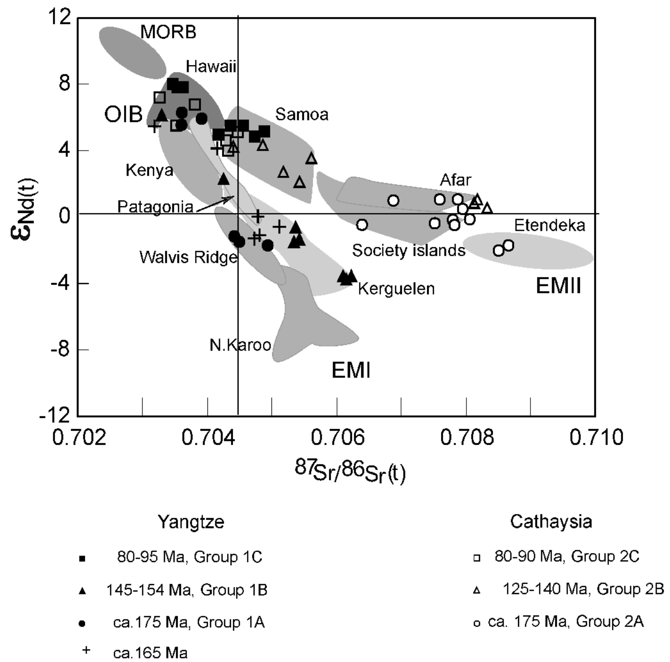

FIG. 6. $^{87}Sr/^{86}Sr(i)$ vs. $\varepsilon_{Nd}(t)$ diagram for Mesozoic mafic rocks of the Yangtze and Cathaysia blocks, showing that Group 1 samples define a mantle array between an OIB field and an EMI-type source, whereas Group 2 samples fall along another array between an OIB field and EMII-type source. Samples with an age of ca. 165 Ma are from Li et al. (1997, 2003).

contamination. Some samples might have been subjected to small degrees of alteration, which can only be determined from petrographic observation and relatively high loss on ignition (LOI; 1.64–3.53% for lavas, and 2.59–5.58% for dikes). However, the absence of reasonable correlations between Na_2O, K_2O, and LOI, and no Ce anomaly, as well as the correlation of Sr-Nd isotopic ratios, suggest that the incompatible elemental and isotopic ratios have not been significantly affected by alteration (Deniel, 1998).

Elemental and isotopic compositions could provide clues about crustal contamination. Group 1 samples plot along the trend of continental lithospheric mantle or crustal contamination in Figure 7. However, Nb/La, $\varepsilon_{Nd(t)}$ systematically decreases and $^{87}Sr/^{86}Sr(t)$ increases with increasing Mg# (Figs. 8B–8D). This observation is contrary to that expected from crustal contamination or AFC (DePaolo, 1981), suggesting that significant crustal contamination for Group 1 samples is unlikely to have occurred during the magma ascent. This phenomenon is absent for the correlation between $^{87}Sr/^{86}Sr$ ratio and K/P for Group 2 samples, and analyses plot within the field of common mantle melts defined by Hart and Staudigel (1989) (Fig. 7), suggesting that Group 2 samples did not undergo the significant crustal contamination. This is also supported by the fact that Nb/La and Zr/Nb ratios for Group 2 samples with similar ages are relatively constant irrespective of SiO_2 contents (Fig. 8A). In summary, the variation of trace-element and isotopic compositions for both groups probably results from source heterogeneities rather than crustal assimilation en route.

Magma fractionation

Most mafic rocks have low Mg# (0.32–0.65) and Ni contents (14–168 ppm), suggesting that they might not represent primary mantle melts, but rather underwent crystal fractionation from parental magmas either in magma chambers or en route to the surface. Decreasing Ni and Cr contents with decreasing Mg# (Fig. 3) also supports the fractionation of olivine and clinopyroxene. In contrast, the

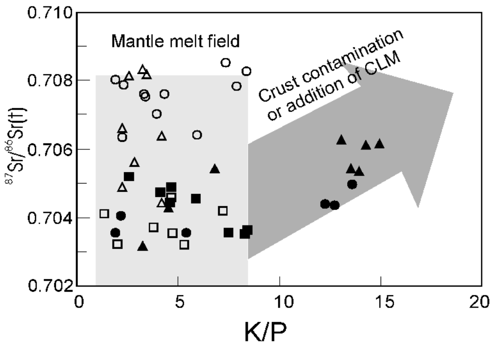

FIG. 7. $^{87}Sr/^{86}Sr(t)$ versus K/P ratio plot for the Mesozoic mafic rocks. The mantle field is from Hart and Staudigel (1989); crust contamination/CLM trend is from Chazot and Bertrand (1993). See Fig. 3A for the symbols.

high-Mg# samples (Mg#>0.65) exhibit high MgO (7.0–18.7%), Cr (123–647 ppm) and Ni (201–1478 ppm) contents (Table 2 and Fig. 3). They also have relatively low Al_2O_3 (9.32–12.64%), TiO_2 (0.58–0.68%) and FeOt (6.9–8.2%), similar to those of the experimental melts of depleted peridotite (Falloon et al., 1988). This suggests that they may represent the primary melts or cumulates. Furthermore, a significantly negative Eu anomaly is rarely present in all the samples, suggesting that plagioclase was not a major fractional phase, consistent with petrographic observations.

Source characteristics

Higher concentrations of incompatible elements in Group 1A and 1B mafic rocks than those in Group 2A and 2B might be related to changes in the depth of the melts (Tatumoto et al., 1992). However, systematic shift in $^{87}Sr/^{86}Sr$ and $^{144}Nd/^{8143}Nd$ ratios between groups (Fig. 6) does not support a scenario that these mafic rocks were generated from variable degrees of partial melting of a homogeneous mantle source (Giannetti and Ellam, 1994). It is more likely that the variations of elemental and isotopic composition reflect source heterogeneities. Based on the negligible crustal contamination scenario discussed above, geochemical characteristics of the mafic rocks with ages of >125 Ma from both groups (Group 1A–B and Group 2A–B), including Nb-Ta and/or Pb anomalies, high $^{87}Sr/^{86}Sr$ ratios and low $\varepsilon_{Nd(t)}$ values, suggest these rocks originated from the continental lithospheric mantle.

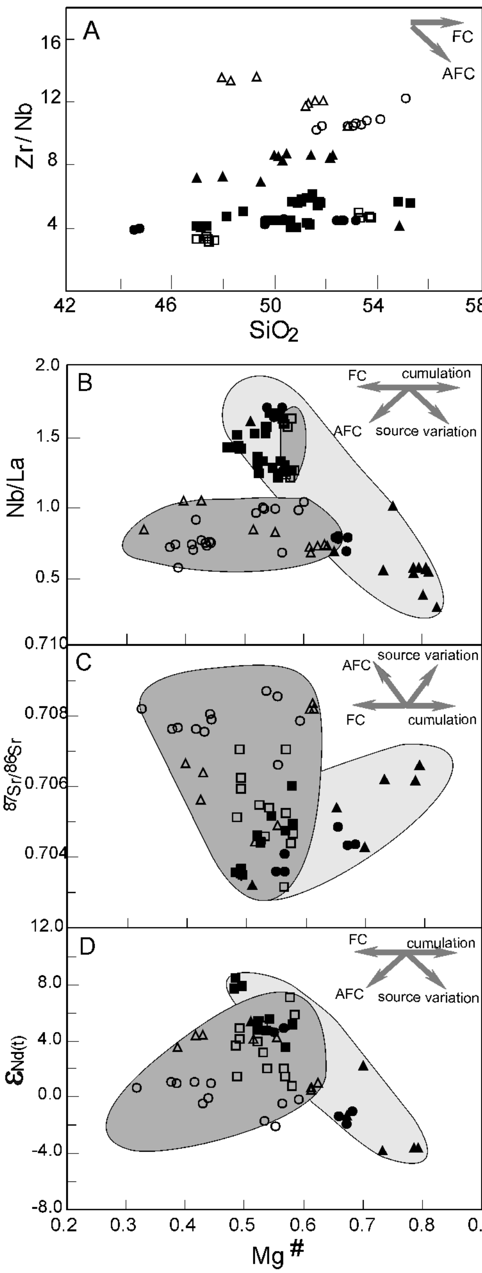

FIG. 8. SiO_2 versus Zr/Nb (A), and Mg# versus Nb/La, $^{87}Sr/^{86}Sr(t)$, and $\varepsilon_{Nd(t)}$ plots (B–D) for Mesozoic mafic rocks of the Yangtze and Cathaysia blocks. See Fig. 3A for the symbols.

According to Humphris and Thompson (1983), Palacz and Saunders (1986), and Weaver (1991), the distinctive characteristics of EMI-type lithospheric mantle are lower $^{143}Nd/^{144}Nd$ ratios than OIB and

EMII, and higher $^{87}Sr/^{86}Sr$ ratios than OIB but lower than EMII. EMII-type lithospheric mantle is characterized by $^{87}Sr/^{86}Sr$ ratios in excess of 0.7065, and intermediate $^{143}Nd/^{144}Nd$ ratios varying between those of OIB and EMI-type mantle (Hart, 1988). The variations of Sr-Nd isotopic compositions (Fig. 6) indicate that three mantle source components are required to account for the Mesozoic mafic petrogenesis in the SCB interior. They correspond to OIB, EMI-, and EMII-like lithospheric mantle sources defined by Zindler and Hart (1986).

Ratios of incompatible elements (e.g., Rb, Ba, Th, Nb, La, Ce, Zr, and Ta) can have much to contribute to the identification of the end members, inasmuch as they are the least susceptible to partial melting and fractional crystallization processes, relative to isotopic ratios (Humphris and Thompson, 1983; Hofmann et al., 1986; Weaver, 1991; Sims and Depaolo, 1997). The Ce/Pb, Nb/U, and U/Pb ratios for Group 1A and 1B samples are in the range of 2.2–7.6, 8.5–16.4, and 0.04–0.18, respectively, lower than those from Group 2A and 2B (5.9–18.9, 7.6–23.1, and 0.16–0.42, respectively). The Group 1C and 2C samples give similar Ce/Pb, Nb/U, and U/Pb ratios (18.7–34.6, 29.2–56.6, and 0.27–0.65) to those of OIB (Ce/Pb = 25 ± 5; Nb/U = 47 ± 10) (Sun and McDonough, 1989; Hofmann et al., 1986).

In Figure 9, the ratios of incompatible elements for both groups plot into two distinct fields that gradually converge. The common field is characterized by Group 1C and 2C samples, similar to those of OIB source. This, together with the preceding discussions (Figs. 2–6), indicate that La/Nb, Ba/Nb, Rb/Nb, Th/Nb and Ba/La ratios in Group 1A–B and Group 2A–B mafic samples are significantly higher than those in an OIB source. Despite an overlapping La/Nb ratio, Group 1A and 1B samples generally have higher Ba/Nb, Rb/Nb, Ba/Th, and Ba/La ratios and lower Th/Nb, Th/La, and Zr/Nb ratios than those in Group 2A and 2B (Table 2). This is in agreement with the fact that EMI-type sources have higher Ba/Nb, Rb/Nb, Ba/Th, and Ba/La ratios but lower Th/Nb, Th/La, and Zr/Nb ratios than EMII-type mantle (Palacz and Saunders, 1986; Weaver, 1991; Tatumoto et al., 1992).

Similarly, when $\varepsilon_{Nd(t)}$ and $^{87}Sr/^{86}Sr(t)$ are plotted against Ba/Nb and La/Nb (Figs. 9E and 9F), these Mesozoic basaltic rocks generally define two different trends. There is a general correlation for Group 1 samples along the OIB end member and the high Ba/Nb, low $\varepsilon_{Nd(t)}$ end-member (EMI-like) array. Group 2 samples fall on the OIB end member and the low Ba/Nb, high $^{87}Sr/^{86}Sr(t)$ end-member (EMII-like) array.

Consequently, the involvement of three main end members might account for the variations of elemental and isotopic ratios for these Mesozoic basaltic samples in the SCB interior. A substantial amount of EMI-type continental lithospheric mantle mixed with the OIB source may contribute to the Group 1 mafic rock source, whereas an EMII-type mantle source, contaminated by an OIB component, may have played an important role in generation of Group 2 mafic rocks. The lithospheric source for Group 1 and Group 2 in the SCB interior, respectively, changed from EMI-and EMII-dominated lithospheric mantle to OIB sources from 175 Ma to 80–95 Ma. This OIB component is the predominant source until 80–95 Ma.

Plate boundary between Yangtze and Cathaysia blocks

The boundary between Yangtze and Cathaysia blocks is generally defined in the literature (e.g., Chen and Jahn, 1998) by the occurrence of the Neoproterozoic Banxi Group, roughly corresponding to the Jinxian-Anhua fault (Fig. 1). The spatial variation of EMI- and EMII-like signatures for Mesozoic mafic rocks around the Chenzhou-Linwu fault may shed some light on the nature of the lithospheric boundary between the Yangtze and Cathaysia blocks.

Group 1 mafic rocks west of the Chenzhou-Linwu fault commonly show an EMI-like isotopic affinity marked by relatively low $^{87}Sr/^{86}Sr$ ratios, LREE enrichment, and high LILE/HFSE ratios. The EMI-type component is known to reside proximally to ancient metasomatized continental lithospheric mantle (Deniel, 1998). In contrast, Group 2 mafic rocks on the east of the Chenzhou-Linwu fault show a prevalent EMII-like isotopic signature, with significantly higher $^{87}Sr/^{86}Sr$ and relatively low LILE/HFSE ratios. An EMII-type component is generally regarded as a signature of modified lithospheric mantle (Humphris and Thompson, 1983; Palacz and Saunders, 1986; Tatsumoto et al., 1992). This indicates that Mesozoic mafic rocks around the Chenzhou-Linwu fault have a distinct affinity to enriched lithospheric mantle and tectonic histories. The Chenzhou-Linwu fault marks the eastern boundary of the EMI-like signature in the Yangtze block and the western boundary of EMII-like signature in the Cathaysia block, and thus represents the Mesozoic lithospheric boundary between both blocks. This boundary is further evidenced by a westward

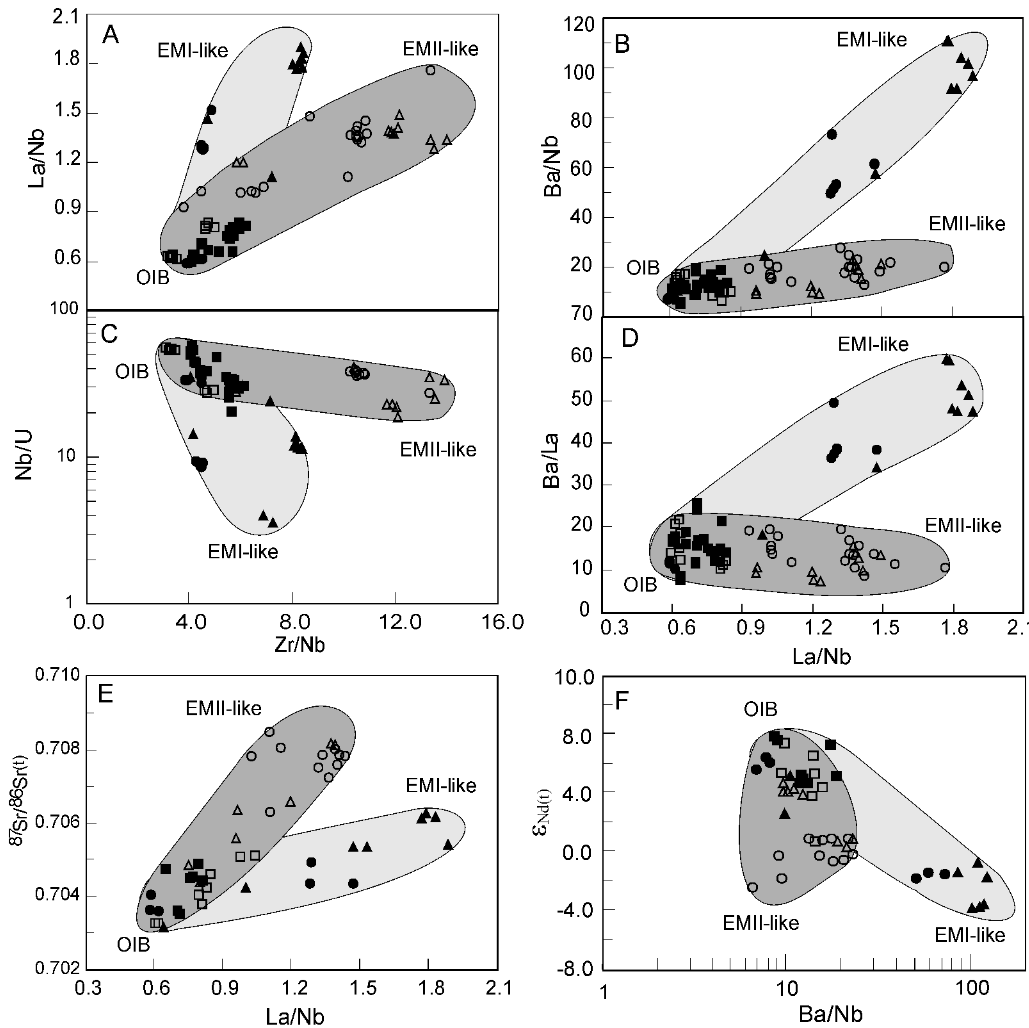

FIG. 9. Correlation among isotopic ratios and ratios of incompatible elements for Mesozoic mafic rocks of the Yangtze and Cathaysia blocks. Group 1 samples plot along the correlation between OIB and a high Ba/Nb, low $\varepsilon_{Nd(t)}$ mantle source (EMI-like), whereas Group 2 samples lie along the correlation between OIB end member and the low Ba/Nb, high $^{87}Sr/^{86}Sr(t)$ mantle source (EMII-like). The symbols are the same as those used in Figure 3A.

verging Early Mesozoic fold and thrust belt, zonal geophysical and geochemical anomalies, and important multi-metal mineralization (Hsü et al., 1990; Qin, 1991; Gilder et al., 1996).

The shoshonite and syenite (126–165 Ma) from western Guangdong and southeastern Guangxi provinces (location 7 in Fig. 1) originated from a mixed source between EMI-like and asthenospheric mantle components (Li et al., 2003), consistent with Group 1 mafic rocks. Li et al (1997) reported that Late Mesozoic mafic dikes (105–140 Ma) from Zhuguangshan in northern Guangdong Province on the east of the Chenzhou-Linwu fault have $\varepsilon_{Nd(t)}$ values of –2.6 to +4.8 and high $^{87}Sr/^{86}Sr$ ratios (0.7050–0.7107), similar to that of an OIB source contaminated with EMII-like component. Therefore, the Wuchuan-Sihui fault probably represents the southern extension of the Chenzhou-Linwu lithospheric boundary (Fig. 1).

The central-west Hunan province, a width of >400 km between the Chenzhou-Linwu fault and the Jinxian-Anhua fault (Fig. 1), is traditionally

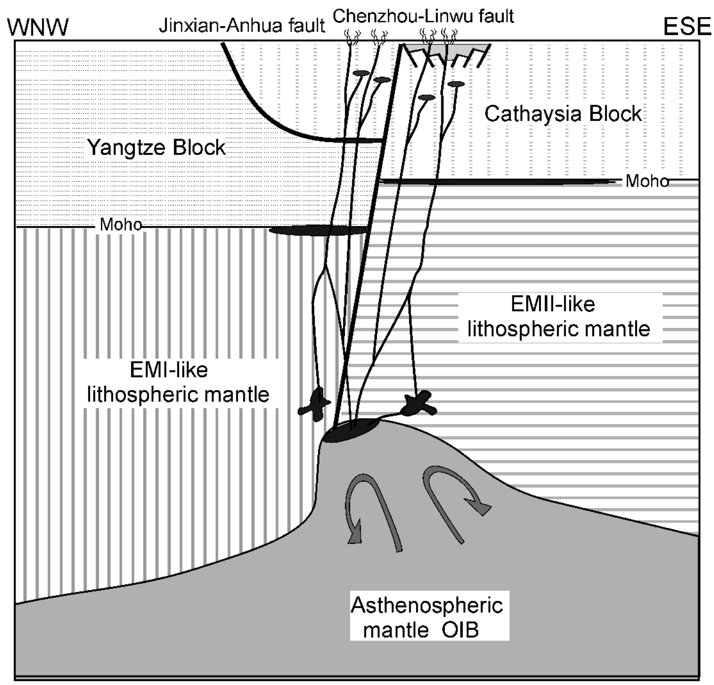

FIG. 10. A conceptual model for Mesozoic lithospheric structure in the SCB interior. Vertical exaggeration is approximately 10×. The Chenzhou-Linwu fault marked the Mesozoic lithospheric boundary between the Yangtze and Cathaysia blocks. The crust of the Cathaysia block overrode the Yangtze block (>ca. 175 Ma). The petrogenesis of the relevant Mesozoic mafic rocks was the result of the lithosphere-asthenosphere interaction in response to intracontinental lithospheric extension, and the contribution of the lithospheric source gradually decreased with time (from EM- to OIB-dominated source until ca. 80 Ma).

considered a part of the Cathaysia block, due to the association of surface structures with the Cathaysia block (Hsü et al., 1990; Li, 1998). Based on the discussions above regarding the lithospheric boundary between both blocks, we here propose a crustal detachment model to account for the decoupling between a deep lithospheric boundary and a near-surface boundary (Fig. 10). That is, the lower part of the lithosphere in west-central Hunan is structurally associated with the Yangtze block, whereas its upper part is attached with the Cathaysia block. In the region, the crust of the Cathaysia block was thrust over the Yangtze block for hundreds of kilometers (>400 km); this thrust event should be no later than ca. 178 Ma. The Neoproterozoic Banxi Group might represent a thrust sheet that experienced large displacement, as proposed by Hsü et al. (1990), and the Jinxian-Anhua fault is merely a near-surface structural boundary between blocks (Figs. 1 and 10).

Constraints on the Mesozoic tectonic evolution of the SCB

The Mesozoic tectonic evolution of the SCB has been long debated. Over the past 20 years, two distinct hypotheses have been postulated. One suggests that Mesozoic tectonic evolution was related to the westward subduction of a Mesozoic Pacific plate, or due to closure of the oceanic basin in the SCB interior (Hsü et al., 1990; Faure et al., 1996; Zhou and Li, 2000). But paleomagnetic evidence has demonstrated that the west-dipping subduction of a Pacific plate occurred no earlier than 125 Ma (Engebretson et al., 1985). This tectonic model has also been challenged by the absence of contemporaneous ophiolite suites, oceanic basins and island-arc magmatism. The second hypothesis advocates that continental rifting and lithospheric extension was the dominant mechanism since the Early Mesozoic, probably even Paleozoic time (Rowley et al., 1989; Gilder et al., 1996; Zhao et al., 1998; Chen and

Jahn, 1998; Li, 2000; Li et al., 2003; Wang et al., 2002, 2003). Our data for Mesozoic mafic rocks have provided some important constraints on the petrogenesis and tectonic evolution of the SCB since the Indosinian event (Li, 1998).

The low-Mg# alkaline basalts in Group 1A rocks show Hawaii OIB-type isotopic and incompatible-element compositions (Figs. 5 and 6) and are regarded as melts of upwelling asthenospheric mantle (Li et al., 2003). The ascending asthenosphere heated, and partially melted, the overlying EMI-type lithospheric mantle. This resulted in the formation of the contemporaneous suite of Group 1A high-Mg# mafic rocks with island-arc-like patterns and EMI-like isotopic signatures. The younger basaltic rocks (Group 1B) might have trapped a substantial amount of EMI-type lithospheric mantle source materials, and as such, exhibit a mixed source between OIB- and EMI-type. In comparison, Group 2A and 2B rocks originated from a hybrid source between OIB and EMII-type lithospheric mantle (Fig. 10). This suggests that the mafic rocks were generated by upwelling asthenosphere under an intra-plate lithospheric extension/thinning regime, rather than in a subduction zone.

Taking into account the occurrence of the Indosinian intra-continental orogenic event (HBGMR, 1988; JBMGR, 1989; Rowley et al., 1989; Li, 1998), it is likely that lithospheric extension and thinning commenced from early-Middle Jurassic in response to post-Indosinian orogenic collapse (Zhao et al., 1998; Wang et al., 2002, 2003; Li et al., 2003), and subsequently dominated the tectonic development of the SCB interior until ca. 130 Ma (Li, 2000). The lithospheric extension hypothesis is also supported by evidence of doming of the contemporaneous metamorphic core complexes (e.g., Wugongshan, Lushan, Mofu, and Jiulingshan), the occurrence of Early Cretaceous granitic magmatism and the formation of redbed fault basins (Faure et al., 1996; Li, 2000; Lin et al., 2000).

As described above, the elemental and isotopic features of both groups seem to converge into the same field toward ca. 80–95 Ma. This convergence field is coincident with the range of OIB source shared by the Cenozoic basalts from eastern China, which most likely originated from an asthenospheric mantle source (Tu et al., 1992; Basu et al., 1991; Chung et al., 1995; Zou et al., 2000). This suggests that Group 1C and 2C mafic rocks in the Yangtze and Cathaysia blocks might have an identical asthenospheric mantle origin (Zindler and Hart, 1986).

Conclusions

The Mesozoic basalts and related mafic dikes with ages of >125 Ma around the Chenzhou-Linwu fault (west block = Group 1; east block = Group 2) exhibit distinct geochemical and isotopic variations. Such new information has provided excellent constraints on the lithospheric boundaries between the Yangtze and Cathaysia blocks and the Mesozoic tectonic evolution of South China. Our conclusions are summarized below.

The K-Ar geochronology indicates that there are three main magmatic episodes around the Chenzhou-Linwu fault, corresponding to ca. 175 Ma, 125–154 Ma, and 80–95 Ma. All the samples of both groups display significantly fractionated LREE, slightly fractionated HREE, and incompatible-element enrichment with variable Nb-Ta anomalies. But Group 1 rocks with ages of >125 Ma commonly have higher LREE and Ba/Nb, Rb/Nb, Ba/Th, and Ba/La ratios, and lower Th/Nb, Th/La, and Zr/Nb ratios, in comparison with those in Group 2 rocks. Group 1 rocks with ages of >125 Ma exhibit $^{87}Sr/^{86}Sr(t)$ = 0.7035–0.7069 and $\varepsilon_{Nd(t)}$ = –3.75 to +6.10, whereas Group 2 rocks have $^{87}Sr/^{86}Sr(t)$ = 0.7075–0.7087 and $\varepsilon_{Nd(t)}$ = –2.04 to +1.05. Group 2 rocks have significantly higher $^{87}Sr/^{86}Sr(t)$ ratios than the contemporaneous Group 1 rocks. Rocks with ages of 80–95 Ma from both groups have similar element and isotope compositions ($\varepsilon_{Nd(t)}$ = +3.99 to +8.00 and $^{87}Sr/^{86}Sr(t)$ = 0.7033–0.7052), similar to those of OIB.

These geochemical and isotopic data suggest that Group 1 rocks with ages of >125 Ma were originated from a mixed source of an EMI-type and an OIB component, whereas Group 2 rocks were derived from an EMII-type with some involvement of an OIB component. Rocks with ages of 80–95 Ma have OIB-dominated signatures. The spatial variations of EMI- and EMII-like signatures for Mesozoic mafic rocks around the Chenzhou-Linwu fault suggest that this fault marked the Mesozoic lithosphere boundary between the Yangtze and Cathaysia blocks. The Jinxian-Anhua fault represented the near-surface boundary between both blocks. The crust of the Cathaysia block might have been thrust westward over that of the Yangtze block at a time no later than ca. 178 Ma, with a displacement of >400 km. The elemental and isotopic data obtained in this study support a crustal detachment collision (>178 Ma) model. The change of source characteristics (from enriched lithosphere mantle source with some OIB component to an OIB-dominated source) is an indication of lithosphere-asthenosphere interaction in response to Mesozoic intracontinental lithospheric extension of the SCB interior.

Acknowledgments

We would like to thank Y. H. Zhang, W. Potma, and H. F. Zhang for their reading of the manuscript and helpful discussions and suggestions. X. Q. Liang and X. Chen are thanked for their help during field work. This study was supported by projects from the Chinese Academy of Sciences (KZCX2-102, KZCX2-SW-117), National Nature Sciences Foundation of China (40002007), and Ministry of Science and Technology of China (G1999043209).

REFERENCES

Basu, A. R., Wang, J. W., Huang, W. K., Xie, G. H., and Tatsumoto, M., 1991, Major element, REE, and Pb, Nd and Sr isotopic geochemistry of Cenozoic volcanic rocks of eastern China: Implications for their origin from suboceanic-type mantle reservoirs: Earth and Planetary Science Letters, v. 105, p. 149–169.

Charvet, J., Lapierre, H., and Yu, Y. W., 1994, Geodynamics significance of the Mesozoic volcanism of southeastern China: Journal of Southeast Asian Sciences, v. 9, p. 387–396.

Chazot, G., and Bertrand, H., 1993, Mantle sources and magma-continental crust interaction during early Red Sea–Gulf of Aden rifting in southern Yemen: Element and Sr-Nd-Pb isotopic evidence: Journal of Geophysical Research, v. 98 (B2), p. 1819–1835.

Chen, J. F., and Jahn, B. M., 1998, Crustal evolution of southeastern China: Nd and Sr isotopic evidence: Tectonophysics, v. 284, p. 101–133.

Chen, P. E., Kong, X. G., Wang, Y. X., Ni, Q. S., Zhang, B. T., and Ling, H. F., 1999, Rb-Sr isotopic dating and significance of Yangshanian bimodal volcanic-intrusive complex from south Jiangxi Province, SE China: Geological Journal of China Universities, v. 5, no. 4, p. 378–382.

Chung, S. L., Jahn, B. M., Chen, S. J., and Chen, C. H., 1995, Miocene basalts in northwestern Taiwan: Evidence for EM-type mantle source in the continental lithosphere: Geochimica et Cosmochimica Acta, v. 59, p. 549–565.

Deniel, C., 1998, Geochemical and isotopic (Sr-Nd-Pb) evidence for plume-lithosphere interactions in the genesis of Grande Comore magmas (Indian Ocean): Chemical Geology, v. 144, p. 281–303.

DePaolo, D. J., 1981, Trace element and isotopic effects of combined wall rock assimilation and fractional crystallization: Earth and Planetary Science Letters, v. 53, p. 189–202.

Engebretson, D. C., Cox, A., and Gordon, R. G., 1985, Relative motions between oceanic and continental plates in the Pacific basins: Geological Society of America Special Paper 206, p. 1–59.

Falloon, T. J., Green, D. H., Hatton, C. J., and Harris, K. J., 1988, Anhydrous partial melting of a fertile and depleted peridotite from 2 to 30 kb and application to basalt petrogenesis: Journal of Petrology, v. 29, p. 1257–1282.

Fan, W. M., and Menzies, M. A., 1994, Geochemistry of volcanic rocks and ultramafic xenoliths from eastern China: Implications for the structure of the lower lithosphere: Geotectonica et Metallogenia, v. 18, p. 332–346.

Faure, M., 1996, Extensional tectonics within a subduction-type orogen: The case study of the Wugongshan dome (Jiangxi Province, southeastern China): Tectonophysics, v. 263, p. 77–106.

Giannetti, B., and Ellam, R., 1994, The primitive lavas of Roccamonfina volcano, Roman region, Italy: New constraints on melting processes and source mineralogy: Contributions to Mineralogy and Petrology, v. 116, p. 21–31.

Gilder, S. A., Gill, J., Coe, R. S., Zhao, X. X., Liu, Z. W., and Wang, G. X., 1996, Isotopic and paleomagnetic constraints on the Mesozoic tectonic evolution of South China: Journal of Geophysical Research, v. 107 (B7), p. 16,137–16,154.

Hart, S. R., 1988, Heterogeneous mantle domains: Signature, genesis and mixing chronologies: Earth and Planetary Science Letters, v. 90, p. 273–296.

Hart, S. R., and Staudigel, H., 1989, Isotopic characteristization and identification of recycled components, *in* Guten, L., and Hart, S. R., eds., Crust/mantle recycling at convergence zones (NATO ASI Series): Dordrecht, Netherlands, Reidel, p. 15–28.

Hawkesworth, C. J., Rogers, N. W., van Calsteren, P. W. C., and Menzies, M. A., 1984, Mantle enrichment processes: Nature, v. 311, no. 27, p. 331–335.

HBGMR (Hunan Bureau of Geology and Mineral Resources), 1988, Regional geology survey in Hunan Province: Beijing, China, Geological Press, 543 p. (in Chinese).

Hofmann, A. W., Jochum, K. P., Seufert, M., and White, W. ., 1986, Nb and Pb in oceanic basalts: New constraints on mantle evolution: Earth and Planetary Science Letters, v. 79, p. 33–45.

Holloway, N. H., 1982, North Palawan Block, Philippines: Its relation to the Asian mainland and role in evolution of South China Sea: American Association of Petroleum Geologists Bulletin, v. 66, p. 1355–1383.

Hsü, K. J., Li, J. L., Chen, H. H., Wang, Q. C., Sun, S., and Sengör, A. M. C., 1990, Tectonics of South China: Key to understanding west Pacific geology: Tectonophysics, v. 183, p. 9–39.

Humphris, S. E., and Thompson, G., 1983, Geochemistry of rare earth elements in basalts from the Walvis Ridge: Implications for its origin and evolution: Earth and Planetary Science Letters, v. 66, p. 223–242.

JBGMR (Jiangxi Bureau of Geology and Mineral Resources), 1989, Regional geology survey in Jiangxi Province: Beijing, China, Geological Press, 1–504 (in Chinese).

Li, X. H., 2000, Cretaceous magmatism and lithospheric extension in southeast China: Journal of Asian Earth Sciences, v. 18, p. 293–305.

Li, X. H., and McCulloch, M. T., 1996, Secular variation in the Nd isotopic composition of Neoproterozoic sediments from the southern margin of the Yangtze block: Evidence for a Proterozoic continental collision in southeast China: Precambrian Research, v. 76, p. 67–76.

Li, X. H., Chung, S. L., Zhou, H. W., Lo, C. H., Liu, Y., and Chen, C. H., 2003, Jurassic intraplate magmatism in southern Hunan–eastern Guangxi: $^{40}Ar/^{39}Ar$ dating, geochemistry, Sr-Nd isotopes and implications for tectonic evolution of SE China: Geological Society of London Special Publication, in press.

Li, X. H., Hu, R. Z., and Rao, B., 1997, Geochronology and geochemistry of Cretaceous mafic rocks from northern Guangdong Province, SE China: Geochimica, v. 26, no. 2, 14–31 (in Chinese).

Li, Z. X., 1998, Tectonic history of the major East Asian lithospheric blocks since the mid-Proterozoic: A synthesis, *in* Flower, M. F. J., Chung, S. L., Lo, C. H., and Lee, C. Y., eds., Mantle dynamics and plate interactions in East Asia: American Geophysical Union, Geodynamics Series, no. 27, p. 221–243.

Lin, W., Faure, M., Monië, P., Schärer, U., Zhang, L., and Sun, Y., 2000, Tectonics of SE China: New insights from the Lushan massif (Jiangxi Province): Tectonics, v. 19, p. 852–871.

Liu, Y., Liu, H. C., and Li, X. H., 1996, Simultaneous and precise determination of 40 trace elements using ICP-MS: Geochimica, v. 25, p. 552–558 (in Chinese).

Middlemost, E. A. K., 1994, Naming materials in the magma/igneous rock system: Earth Science Review, v. 37, p. 215–224.

Morrison, G. W., 1980, Characteristics and tectonic setting of the shoshonite rock association: Lithos, v. 13, p. 97–108.

O'Reilly, S. Y., and Griffin, W. L., 1996. 4-D lithospheric mapping: Methodology and examples: Tectonophysics, v. 262, p. 3–18.

Palacz, Z. A., and Saunders, A. D., 1986, Coupled trace-element and isotope enrichment in the Cook-Austral-Samoa islands, southwest Pacific: Earth and Planetary Science Letters, v. 79, p. 270–280.

Qin, B. H., 1991, Deep-seated structure beneath Hunan Province revealed by the Taiwang-Heishui geotraverse: Hunan Geology, v. 15, 89–96 (in Chinese with English abstract).

Qiu, Y. M., Gao, S., McNaughton, N. J., Groves, D. I., and Ling W. L., 2000, First evidence of >3.2Ga continental crust in the Yangtze craton of South China and its implications for Archean crustal evolution and Phanerozoic tectonics: Geology, v. 28, p. 11–14.

Rowley, D. B., Ziegler, A. M., and Nie, G., 1989, Comment on "Mesozoic overthrust tectonics in South China": Geology, v. 17, p. 384–386.

Sims, K. W. W., and DePaolo, D. J., 1997, Inferences about mantle magma sources from incompatible element concentration ratios in oceanic basalts: Geochimica et Cosmochimica Acta, v. 61, p. 765–784.

Sun, S. S., and McDonough, W. F., 1989, Chemical and isotopic systematics of oceanic basalts: Implication for mantle composition and process, *in* Sauders, A. D., and Norry, M. J., eds., Magmatism in the ocean basins: Geological Society of London Special Publication 42, p. 313–345.

Tatumoto, M., Basu, A. R., and Huang, J. W., 1992, Sr, Nd, Pb isotopes of ultramafics in volcanic rocks of eastern China: Enriched components EMI and EMII in subcontinental lithosphere: Earth and Planetary Science Letters, v. 113, p. 107–128.

Taylor, S. R., and McLennan, S. M., 1985, The continental crust: Its composition and evolution: Oxford, UK, Blackwell.

Tu, K., Flower, M. F. J., Carlson, R. W., Xie, G. H., Chen, C. Y., and Zhang, M., 1992, Magmatism in South China Basin: 1. Isotopic and trace element evidence for an endogeneous Dupal mantle component: Chemical Geology, v. 97, p. 47–63.

Wang, Y. J., Fan, W. M., Guo, F., and Li, H. M., 2002, U-Pb dating of early Mesozoic granodioritic intrusions in southeastern Hunan Province and its petrogenetic implication: Science in China (series D), v. 3, p. 270–280.

______, 2003, Geochemistry of Early Mesozoic potassium-rich dioritic-granodioritic intrusions in southeastern Hunan Province, South China: Petrogenesis and tectonic implications: Geochemical Journal, in press.

Weaver, B. L., 1991, The origin of ocean island basalt end-member compositions: Trace element and isotopic constraints: Earth and Planetary Science Letters, v. 104, p. 381–397.

Xu, J. W., Ma, G., Tong, W. X., Zhu, G., and Lin, S., 1993, Displacement of the Tancheng-Lujiang wrench fault system and its geodynamic setting in the northwestern Circum-Pacific, *in* Xu, J., ed., The Tanchang-Lujiang wrench fault system: John Wiley and Sons, p. 51–74.

Zhao, Z. H., Bao, Z. W., and Zhang, B. Y., 1998, The geochemistry of Mesozoic basalts in south Hunan

Province, South China: Science in China (series D), v. 28 (suppl.), p. 7–14.

Zhou, X. M., and Li, W. X., 2000, Origin of Late Mesozoic igneous rocks in Southeastern China: Implications for lithosphere subduction and underplating of mafic magmas: Tectonophysics, v. 326, p. 269–287.

Zindler, A., and Hart, S. R., 1986, Chemical geodynamics: Annual Review of Earth and Planetary Science, v. 14, p. 493–571.

Zou, H. B., Zindler, A., Xu, X. S., and Qi, Q., 2000, Major, trace element, and Nd, Sr and Pb studies of Cenozoic basalts in SE China: Mantle sources, regional variations, and tectonic significance: Chemical Geology, v. 171, p. 33–47.